AN ANALYSIS OF RADIATION-INDUCED STRESSES OF A GRAPHITE CENTRAL
REFLECTOR IN A PEBBLE BED FLUORIDE SALT-COOLED REACTOR CORE

By

Madicken Munk

A Report Submitted to in Partial Completion for the Degree of
Master of Science
in Nuclear Engineering
at the Graduate Division of
University of California Berkeley

Winter 2013

Under the Guidance of:
Professor Ehud Greenspan
Professor Per Peterson
Professor Massimiliano Fratoni

Report UCBTH-14-008

Abstract

The theory and process behind evaluating the lifetime of a key reactor component in the Pebble-Bed Fluoride Salt-Cooled High Temperature Reactor (PB-FHR) is detailed. Development of a large-scale, commercial PB-FHR design is currently being spearheaded by the University of California-Berkeley (UCB) as a part of the FHR-Integrated Research Project (FHR-IRP), a joint collaboration between UCB, the University of Wisconsin-Madison, and MIT. The design developed at UCB involves an annular PB-FHR core with a graphite central reflector that will be utilized for reactivity control and coolant insertion. Examining the time limitation of the geometric integrity of the central reflector is key in evaluating the feasibility of such a design.

A study using the FEM program COMSOL multiphysics was used to ultimately determine the lifetime of this central reflector. The damage rate and fluence deposition were first calculated using MCNP5. Using experimental data, a dimensional change was imposed on the differential volumes within the mesh given their fluences. This dimensional change then induced stresses in the model, which were quantified with COMSOL. This was done using a pseudo-temperature distribution, as COMSOL is not readily adaptable to a direct approach neutron damage analysis. As such, the model does not calculate the volume changes based on the actual mechanisms of radiation damage, but instead uses the experimental data to impose the dimensional changes. This method was used to determine a lifetime for a test case, a large monolithic central reflector, and a central reflector assembled from smaller graphite blocks with a more complex geometry.

This method could be used as a first-order estimate of component lifetime for any material where the dimensional changes as a function of neutron fluence are known. Most data is also temperature dependent, so choosing experimental data relevant to one's system is extremely important for a meaningful result. Other physics, including, but not limited to creep, thermal stress, structural loading, and bending may also be relevant to other studies, but were not examined for this project.

Acknowledgements

The work presented in the following pages could not have been completed without the help and guidance of a large number of individuals, and I would like to take the time and space to mention them here.

First, I would like to acknowledge both of my advisors, Professors Ehud Greenspan and Per Peterson. I thank you both for sharing even small portions of your wealth of knowledge with me. Someday I hope to have learned just a fraction of what you know. Professor Greenspan, thank you for challenging me to think more deeply about the physics and theory behind the analyses that I have performed, and always pushing me to understand the importance of *why*. Professor Peterson, thank you for first introducing me to this topic, and helping me to expand my field of expertise. Thank you also for your financial support throughout my graduate studies, and including me on the FHR-IRP.

Secondly, to Tommy Cisneros, without whose input and encouragement I would have not begun working on the FHR project as early as I did. Tommy, you helped me learn the future of reactor physics, and I thank you for that.

I would also like to thank Professor Max Fratoni, who took the time to provide valuable critique and input on this work.

Finally, this work could not have been completed without the support and guidance of so many of the graduate students and postdocs here at UCB. Lakshana Huddar, thank you for taking the time to help me learn COMSOL and also to debug the countless errors and erraneous results that I had throughout this project. David Krumwieide, who also was an invaluable resource on COMSOL issues as well as CAD issues, and who provided incredible support in providing me the CAD models for this analysis. Both Lakshana and David provided me with incredible moral support and encouragement throughout my time on this project. Jeff Seifried, for his continual sanity checks on my work, as well as his continual guidance in all things reactor physics. Lastly, to my friends; Katy Huff, Denia Djokic, George Zhang, Alejandra Jolodosky, and so many others. Last I would like to thank my family; Donald Munk, Romana Voigt, Asbjorn Munk, Caitlin Thompson. Without your support I would not be where I am today.

1. Introduction

Fluoride salt cooled, high temperature reactors (FHRs) provide a potentially attractive technology to deliver safe, high-temperature nuclear power. The FHR Integrated Research Project (FHR-IRP) is a joint collaboration between UCB, the University of Wisconsin-Madison, and MIT to investigate FHRs as a reactor concept. Each university has a separate and distinct role on the project; UCB specifically focuses on neutronics and thermal hydraulics studies for FHRs. To perform this work UCB also developed a preconceptual design for pebble bed FHR. A series of white papers have been published outlining the progress of the FHR-IRP [1,2, 15, 16].

The variant of the FHR currently under development at UCB is a 236 MWth Mark 1 Pebble Bed FHR (Mk1 PB-FHR) [21]. The pebbles in this design are positively buoyant in the Flibe, a fluoride lithium beryllium eutectic salt. The flibe is enriched in Li-7, as Li-6 is a significant neutron absorber and will adversely affect the burnup optimization in the core. The flibe absorbs heat from the pebbles, which are continuously recirculated through the core. Some pebbles include fuel, but others are inert graphite pebbles used to shield the outer reflector from radiation damage. This PB-FHR design is also an annular core—meaning that there is an inner, central reflector. This reflector not only minimizes power peaking in the core by spreading the power over a larger cross-sectional area, but it also provides reactivity control, which is extremely important for the reliability and control of the FHR during operation. The central reflector houses the control rod channels, which will be used for reactivity control. As such, it is not a viable option to add an inert graphite pebble blanket to protect this reflector, as the graphite pebbles will reduce the effectiveness of the control rods by increasing the distance between the strongly neutron absorbing control rods and the active, neutron-producing fuel. However, the central reflector will see extremely high neutron fluences over the lifetime of the core. All materials change over time under neutron irradiation conditions, and graphite is not excluded. It is extremely important, then, to determine at which point in the reactor lifetime that the structural and physical integrity of the central reflector will be compromised, which may include breakage, excessive physical deformation, or by blocking the control rod channels.

This report documents the background, methodology, and theory used to evaluate the PB-FHR central reflector neutron damage rates and lifetime. It should be noted that this is a first-order approach to the problem, and further into the PB-FHR design process a more comprehensive analysis that includes full core lifetime physics should also be performed.

2. Background

Several previous studies have investigated the design optimization of fuel and core of the Mk1 PB-FHR [12]. However, these analyses were optimized for thermal-hydraulic, neutronic, and some economic feedback; a more refined analysis of key reactor components will be required for a more detailed look at component replacement frequency. The inner central reflector of the PB-FHR will see some of

the highest neutron fluxes in the core, which will expose the central reflector to high damage rates and place a limitation on the lifetime of this key component. The central reflector is integral to the safe and controlled operation of the PB-FHR because it provides coolant flow paths to create cross flow in the core and it houses the control rod channels, which are required for reactivity control during full-power operation, as well as reactivity control for startup and shutdown. The geometric integrity of these channels is required for control rod insertion, and determining a central reflector lifetime based on material limitations and core conditions that will compromise the central reflector's integrity is essential for the evaluation of the feasibility of a PB-FHR reactor design.

2.1 Nuclear Grade Graphite

The PB-FHR central reflector serves the neutronic purpose of reflecting neutrons back into the pebble-filled core. This is accomplished with a solid material with low atomic mass, low probability of neutron absorption, and with low chemical reactivity in the salt. Graphite, due to its extensive use in high temperature gas cooled reactors (HTGRs) [10, 14, 18, 19, 24, 25, 31] is an attractive choice for use in FHRs as well. Nuclear grade graphite (NGG) is a variant form of graphite with very low impurity levels. For the purposes of the central reflector, an isotropic graphite is also important. Isotropic graphite is characterized by having similar material properties in the parallel and perpendicular planes (usually an isotropy ratio is defined as the ratio between thermal expansion coefficients), where the parallel and perpendicular planes are measured in reference to the forming axis [10].

To create a NGG, usually the manufacturer starts with coke. Coke is a heat-treated byproduct of either petroleum or coal processes (petroleum coke or pitch coke), which, at high enough temperatures, separates the high Z impurities from the low Z carbonaceous solid. The coke is crushed and then formed with either extrusion, molding, vibrational molding, or isostatic pressing [24, 25, 27]. This solid is then baked at a high temperature for graphitization, and the material forms a more stable lattice structure. Depending on the molding method, the graphite crystals will preferentially align, which will lead to anisotropic material properties. This anisotropy can be minimized by having very medium to fine grain size from the coke, and the processing methods can also influence this outcome. Fine grained graphites formed with isostatic pressing can produce near-isotropic NGGs [4].

Depending on the purity of the NGG, applications of the material might be limited to certain areas of the core. Very high purity NGGs are optimal for high fluence regions in the core, as they will have very low neutron absorption and activation. Pitch coke formed NGGs are often candidates for high-fluence regions of the core as they are produced in a gaseous phase, and so have lower impurity levels than the petroleum coke blended graphites [7].

It is important to note that while all NGGs are graphite, their formation methods and source material ultimately will influence their material properties. The material properties of different NGGs range significantly. Density ranges from $1.7 g/cm^3$ to $1.9 g/cm^3$. The thermal expansion coefficient and Young's modulus vary

up to 10%, and their strengths (tensile, bending and compression) vary orders of magnitude. For reference, see Table 3.1.1

Ultimately, IG-110 NGG was chosen as the preliminary graphite with which to analyze the radiation-induced stresses in the central reflector. This choice was primarily based on the availability of data on the material properties of IG-110 at the temperature regimes that the PB-FHR will have, as well as the breadth of data of material properties over a large range of fluences. With data that potentially spans fluence levels not seen in the central reflector for several years, the amount of data extrapolation will be minimized.

2.2 Heavy-Ion and Neutron Damage in Materials

Understanding the mechanisms and theory behind radiation damage is a large and well-explored subfield of materials science. The Kinchin-Pease model was one of the first to illustrate damage propagation instigated by neutron damage in materials. An energetic neutron will travel into a material and interact with a lattice atom. If the neutron energy is larger than the displacement energy (E_D) of the material, it will knock the atom out of its lattice site, creating a lattice vacancy. This atom is then called the primary knockon atom (PKA), and if it does not move to another vacant lattice site it will become an interstitial defect. The displacement energy is the energy required to knock an atom out of a lattice site. It should be noted that this energy is different and not equal to the binding energy of the atom in the lattice. For Graphite E_D is ~24eV to 60eV [4], and E_B is ~7eV. The PKA will then have a kinetic energy that was imparted from the interacting particle, in this case a neutron. Due to its much larger size, and that it has been knocked out of its energetically stable lattice site, it will interact almost immediately with other atoms in the surrounding lattice, creating other atomic displacement atoms, or secondary knockon atoms (SKAs). This continual passing of kinetic energy to lattice atoms and knocking them out of lattice sites is called a displacement cascade. Displacement cascades create large amounts of vacancy and interstitial defects, as well as multidimensional material defects. In this process, there will be a wake of displacements created as the incident particle, PKA, and SKAs continue through the material from the initial interaction. Early on in this process, one can imagine a large cluster of vacancies bounded by a layer of lattice atoms with a large population of interstitial defects. The first model of this "displacement spike" can be found in Fig. 2.2.1 After some time, diffusion will move both of these defects and the material will return to a more energetically favorable state. However, this process begins almost instantaneously, and so Fig 2.2.1 was revised to a more realistic FIGURE 2.2.2 [29].
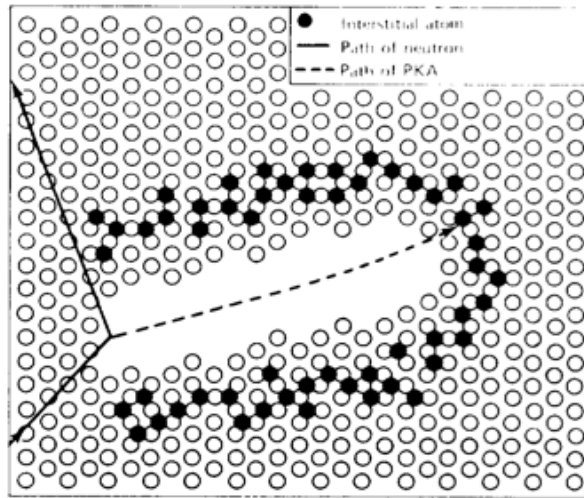
Figure 2.2.1: Original displacement cascade model [29]
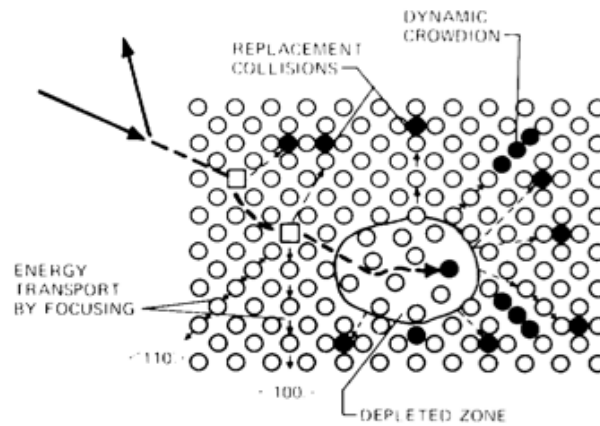
Figure 2.2.2: Later model for displacement spike [29]

Radiation damage is usually expressed in units of displacements per atom, or DPA. This is a numerical expression of the displacement cascade described in the previous paragraphs. The total number of displacements created for an atom of kinetic energy T can be found by:

$$N_D = \frac{T}{2E_D}$$

where E_D is the displacement energy of the atom in the lattice material. Note that the displacement energy has a significant range, and so the calculated N_d can vary significantly (in the case of graphite, almost 50%). However, in a reactor system it is more useful to consider the damage imparted by the neutron flux in the reactor. First consider the total scattering reaction rate per unit volume of neutrons in the material:

$$R_{scatters} = \sigma_s N \phi$$

which gives the total scatters in the material per second. Multiplying this by the displacements created per neutron scattered, N_D, we have the total number of displacements created per cm^3 per second:

$$R_{displacements} = R_{scatters} * N_D$$

Integrating this over time and dividing by the number density of the material, we have an expression for DPA, or the average number of times each atom in the material has been displaced:

$$DPA = \int \frac{R_{displacements} dt}{N}$$

Assuming that the cross section, number density and flux are constant with time:

$$DPA = \frac{R_{displacements} * t}{N}$$

Bringing everything together:

$$DPA = \frac{\sigma_s N \phi t N_D}{N} = \sigma_s \phi t N_D$$

In terms of fluence, or the multiple of flux and time:

$$DPA = \sigma_s \Phi N_D$$

And in an energy dependent form:

$$DPA = \iint \sigma_s(E,t) \phi(E,t) N_D(E,t) \, dt dE$$

Integrating over time, the DPA can be written in terms of an energy-dependent fluence (This assumes that N_D and σ_s do not change with t):

$$DPA = \int \Phi(E) \sigma_s(E) N_D(E) \, dt dE$$

For a reactor system, the energy-dependent integral form of DPA is necessary, as the neutron flux is varies significantly with neutron energy. DPA is more often used as a damage measurement for ion beam irradiation, as the beam is monoenergetic and the variables are approximated as time-independent. While literature may express experimental results for ion-beam irradiation as a function of DPA, it is also common to express damage results as a function of fast fluence for reactor systems. The fast fluence is defined as:

$$\Phi = \int_{E_{fast}}^{\infty} \int_{0}^{t} \phi(E, t) \, dt \, dE$$

Where E_{fast} is the lower limit of "fast" neutrons. This value ranges throughout the literature, but is usually in the range of 0.1 MeV to 0.5 MeV. For this study, choosing to represent damage as a function of fast fluence instead of DPA was chosen because it had less variation in the literature for its calculation. Note that DPA and fluence are expressed in different units: displacements/atom and particles/cm^2, respectively. Relations between the two have been correlated [10, 27, 31], but are dependent on the reactor system in question, as well as on the arbitrarily chosen displacement energy.

2.3 Response of Graphite to Neutron Damage

While the previous section described the generic treatment of radiation damage in materials, the reaction of different materials to radiation damage varies significantly. In a material, once an atom is knocked out of its lattice site, the atom's fate can either be that it finds a vacancy or grain boundary and "heals" out, or it will be an interstitial defect—an atom not bound in the lattice, but still in the crystal. Because the nature of graphite, bonds are in "sheets", with strong bonds along the sheet and a weaker bond between the sheets. The interstitial defects will preferentially move along sheets, but not across them. Of those that do not heal out, many coalesce to form a new "sheet" of graphite, creating a dislocation loop. The mobility of the interstitial graphite atoms is highly dependent on the neutron energy spectrum, the temperature of irradiation, and the number of defects in the material. At high temperatures, interstitials are highly mobile and a large proportion of them will heal out. In general, the formation of interstitial defects will swell the graphite perpendicular to the planar sheets, and the production of vacancies in the sheets will tend to shrink the graphite in the parallel direction [4, 7, 19].

The planar structure of the graphite bonds make it such that graphite is unique among reactor structural materials in its response to radiation damage. Most materials begin to swell under neutron irradiation due to the production of defects in the material. Graphite responds to neutron irradiation by first shrinking, and then swelling. The nature of this response has been studied thoroughly [7], but is still not completely understood. The foregoing theory is that the interstitials cause cross-linking of the planes, which caused the planes to bend, fragment, and then tilt [7]. The magnitude of this effect increases with temperature, but also occurs at greater fluences. The response of a particular grade of nuclear graphite to fast neutron damage is illustrated in Fig 2.3.1. Because this particular grade of graphite is relatively isotropic, with no long-range sheet structure, the dimensional change is equal in all three directions.
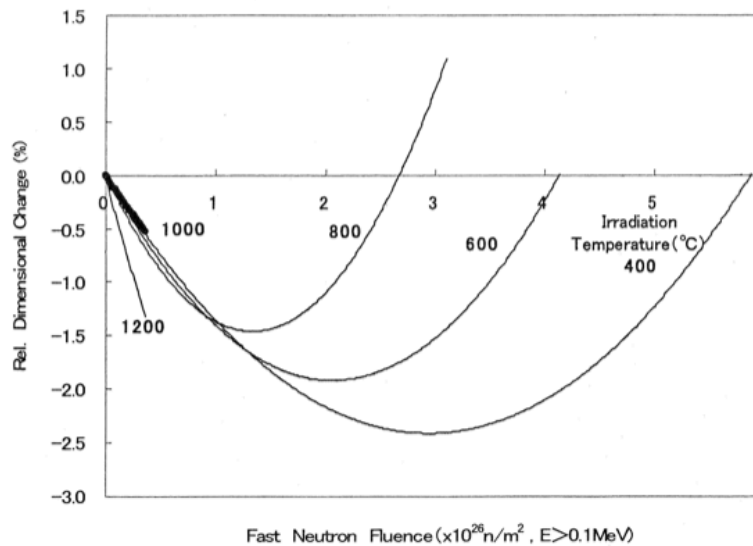
Figure 2.3.1: Dimensional Change of IG-110 Graphite at Various Irradiation Temperatures [31]

The presence of atomic impurities in materials also influences how likely it will be for a defect to heal out of the system. This is because the atomic impurities create energetic discontinuities in the lattice, which hinders defect migration. With hindered dislocation motion, the shrinkage and swelling of graphite is likely to be magnified, creating a stress profile with larger magnitudes, and a shorter lifetime in the reactor system.

Future design iterations of the central reflector of the PB-FHR ultimately will be designed to minimize the radiation-induced stresses while maintaining control rod and coolant channel functionality. However, starting the analysis with a baseline design will inform the design process and quantify the relative effect of various design iterations on minimizing radiation-induced stresses. As such, the baseline design will be the most simplified version of the central reflector, with as much geometric simplicity as possible.

3. Methodology

The objective of this project is to quantify radiation-induced stresses in the Mk1 PB-FHR graphite central reflector using readily available structural mechanics codes. The following section will outline the methodology by which this was achieved, and what potential limitations this analysis might have. This project primarily used two code systems: MCNP5 and COMSOL multiphysics. COMSOL multiphysics has a vast range of applicability in structural mechanics, but also has heat transfer and fluid mechanics modules. Previous modeling has been performed by the Thermal-Hydraulics (TH) group at UC Berkeley using COMSOL's heat transfer and fluid mechanics modules. An analysis using the physics of all three phenomena can be readily implemented in the future by continuing analysis in COMSOL.

Utilizing the experience base of COMSOL in the TH group also aided in a faster and more thorough analysis of this problem.

While COMSOL is the primary tool used in directly calculating the radiation-induced stresses of the central graphite reflector, it requires input on the state of the central reflector while it is in the core. In short, it requires some information on the quantity of neutron damage that the central reflector has received. MCNP5 has an extensive experience base worldwide, and previous analyses of the PB-FHR [10] have been performed with it, so continuing to perform neutron transport calculations with its use was a logical step. As outlined in Section 2, the neutron damage of the central reflector is dependent on the fast neutron fluence. The fast flux is readily calculated with an f4 mesh tally in MCNP5, and then the stress state at different points in the reactor lifetime can be evaluated by multiplying the flux by the residence time of the central reflector in the core.

With a known fast fluence distribution over the central reflector, data from the literature on the dimensional change response of graphite as a function of fast fluence can be incorporated into the COMSOL model. This distribution of dimensional changes on a large component then induces a stress distribution, which at some point will limit the reflector's lifetime. The stress distribution can be calculated by incorporating the dimensional change data in COMSOL, as well as various material properties required to perform the calculation. The following sections outline the data required and methodology used to perform these steps and evaluate the central reflector lifetime.

3.1 Material Properties

In its most basic form, stress is related to strain by the following equation:

$$\sigma = E\epsilon$$

where σ is the stress, E is young's modulus, or the elastic modulus, and ε is the strain. Material properties of unirradiated graphite are in Tables 3.1.1-3.1.3, from various sources.

Table 2
Physical and mechanical properties of some common nuclear graphites (Burchell 1999).

Grade	Source	Forming method[a]	Bulk density (gcm⁻³)	Elastic modulus[b] (GPa)	Strength[b] (MPa) Tensile	Bend	Compression	Thermal conductivity[b] (Wm⁻¹K⁻¹)	CTE[b] (10⁻⁶K⁻¹)
PGA	UK	E	1.74	12/5	17/11	19/12	27/27	200/109	0.9/2.8
SM2-24	UK	M	1.7	8/8.5	12	19	47		
Pitch-coke	UK/France	E	1.8	13/10	25/17	32/26	70/63	130/135	4/3.8
IM1-24	UK	M	1.81	11	27.5	23	70	131	4.3
AGOT	USA	E	1.7	10/8	10/9	16/13	41/41	227/138	2.2/3.8
H-451	USA	E	1.75	11/9.6	15/13	20/24	60/60	150/135	3.5/4.5
ASR-1RS	Germany	M	1.78	9.9/9.2	15/14	26/232	67/63	125	4.7/4.9
IG-110	Japan	I	1.75	10	25	34	71	124/138	4/3.6
TSX	USA	E	1.7	14/3.8	25/7				1/4
GR-280	Russia	E	1.72	6.5/5	7.6/6		34/24	103/89	3.2/4.9
GR2-125	Russia	E	1.85	12/8.5	15/8		59/59	160/100	3.9/5.2

a E, extruded; M, molded; I, isostatic pressing. b Parallel/perpendicular to the forming axis.

Table 3.1.1: Material Properties of Common NGGs [4]

Typical virgin material property for isotropic graphite

Material property of isotropic graphite	Values
Density (g/cm^3)	1.81
Mean coefficient of thermal expansion (CTE) (°C)	4.35×10^{-6}
Poisson's ratio	0.2
Dynamic Young's modulus (GPa)	10

Table 3.1.2: Typical virgin material properties for Isotropic Graphite [32]

Table 2 Typical properties of several well-known grades of nuclear graphite

Property	PGA		CSF		Gilsocarbon		IG-110		H451	
Production method	Extruded		Extruded		Press-molded		Iso-molded		Extruded	
Direction	WG	AG	WG	AG	WG	AG	WG	AG	WG	AG
Density (g cm^{-3})	1.74		1.66		1.81		1.77		1.76	
Thermal conductivity (W m^{-1} K)	200	109	155	97	131		116		158	137
CTE, 20–120 °C (10^{-6} K^{-1})	0.9	2.8	1.2	3.1	4.3					
CTE, 350–450 °C (10^{-6} K^{-1})							4.5			
CTE, 500 °C (10^{-6} K^{-1})			1.5	3.5			3.6	4.0	4.4	5.1
Young's modulus (GPa)	11.7	5.4	8.0	4.8	10.9		9.8		8.51	7.38
Poisson's ratio	~0.07				0.21		0.14		0.15	
Strength, tensile (MPa)	17	11			17.5		24.5		15.2	13.7
Strength, flexural (MPa)	19	12			23.0		39.2			
Strength, compressive (MPa)	27	27			70.0		78.5		55.3	52.7

Table 3.1.3: Properties of NGGs [25]

Note the significant variation in material properties for various NGGs, and also the significant variation in densities for different (and even the same) NGGs. The choice of IG-110 graphite for this analysis was elaborated upon in previous sections. The availability of fluence-dependent properties was a limiting factor for these analyses, but H-451 also had a substantial dataset on fluence-dependent properties [10]. Note the difference in tensile strengths between the two materials, however. IG-110 has a greater tensile and a greater compressive strength than H-451 graphite, but a comparable elastic modulus. Given that the tensile strength, which is the limiting factor for failure (see section 3.5), is 40% greater for IG-110, it appears to be a more attractive candidate for our first analysis. However, with further iterations on this research it may be revealed that H-451 graphite performs the best overall when other factors, like creep (which reduces stresses over time), are also accounted for.

It has been evident throughout the previous sections of this paper that the graphite will undergo dimensional changes as a result of neutron irradiation. However, several material properties are also fluence-dependent [10,31], and were accounted for in the model.

Of primary importance, the elastic modulus, or Young's modulus (stated in the previous equation) relates stress and strain, and varies as a function of radiation damage [31], as illustrated in Figure 3.1.1.
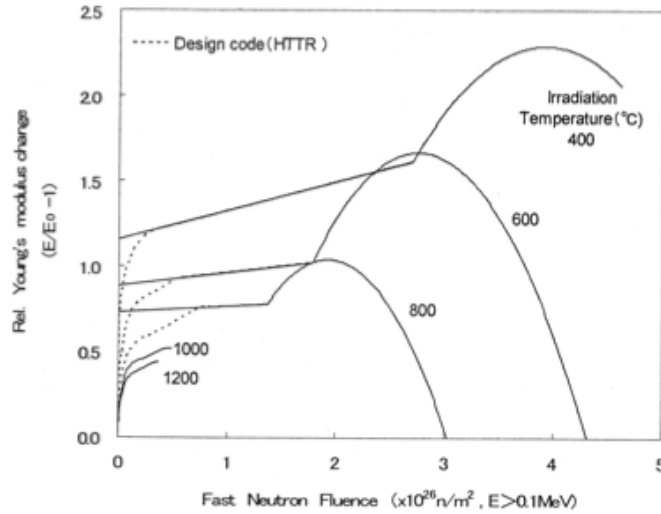
E₀: Longitudinal elastic modulus of unirradiated IG-110 graphite
E : Longitudinal elastic modulus of irradiated IG-110 graphite

Figure 3.1.1 Change in Young's Modulus as a Function of Fast Neutron Fluence [31]

Other material properties that vary as a function of fluence were the thermal conductivity (Fig 3.1.2), the ultimate tensile strength of the material (Fig 3.1.4) , and the thermal expansion coefficient (Fig 3.1.3).
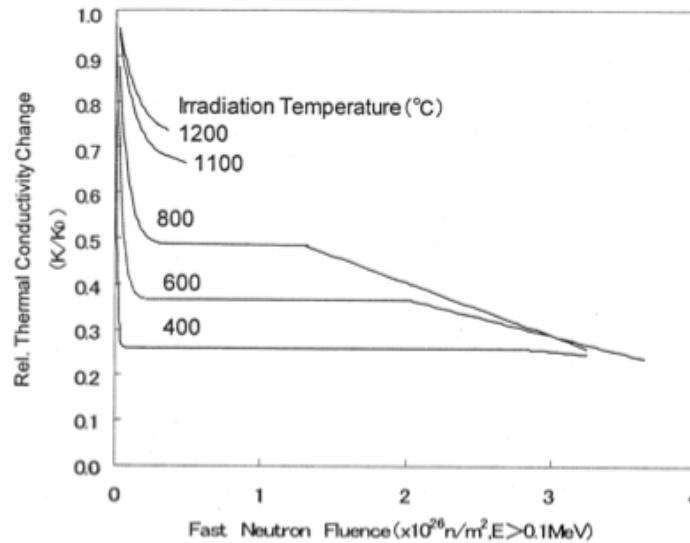
K_0 : Thermal conductivity of unirrradiated IG-110 graphite at the irradiation temperature
K : Thermal conductivity of unirrradiated IG-110 graphite at the irradiation temperature

Figure 3.1.2: Change in Thermal Conductivity as a Function of Fast Neutron Fluence [31]
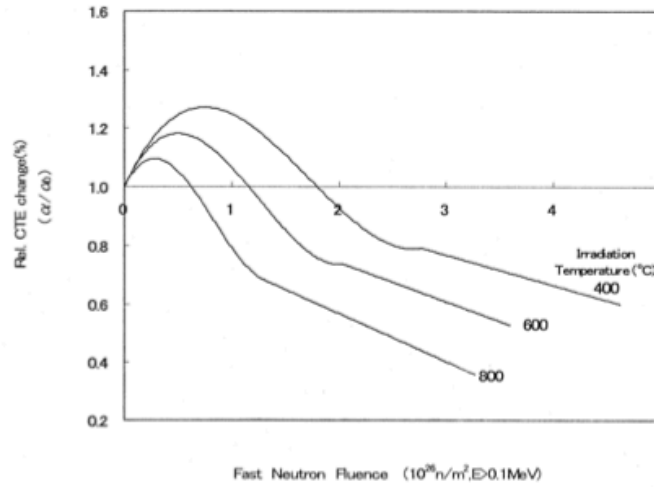
CTE: Coefficient of thermal expansion

($\overline{\alpha_0}$: Average CTE of unirradiated IG-110 graphite from 20 °C to irradiation temperature)

($\overline{\alpha}$: Average CTE of unirradiated IG-110 graphite from 20 °C to the irradiation temperature)

Figure 3.1.3: Change in Coefficient of Thermal Expansion as a Function of Fast Neutron Fluence [31]
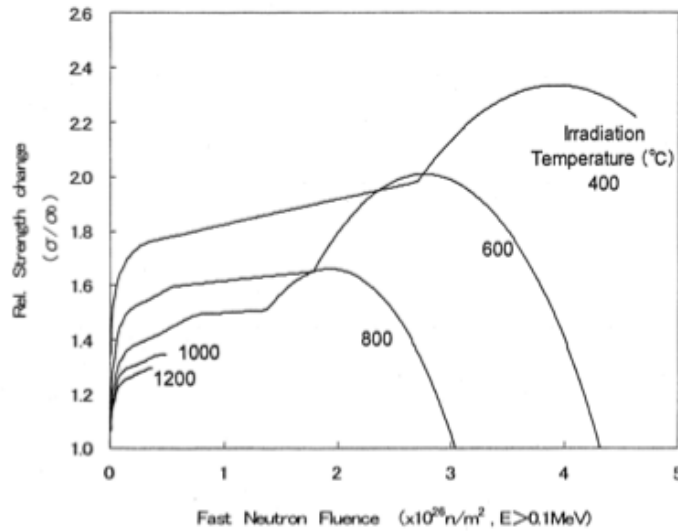
σ_0 : Tensile strength of unirradiated IG-110 graphite

σ : Tensile strength of irradiated IG-110 graphite

Figure 3.1.4: Change in Tensile Strength as a Function of Fast Neutron Fluence [31]

Though the thermal conductivity and coefficient of thermal expansion are fluence-dependent properties, they were not accounted for in the COMSOL model. The reason for their exclusion was primarily due to the fact that a temperature distribution was imposed on the model to simulate radiation-induced stress. As a result, adding the fluence-dependent thermal conductivity would be useful for heat-transfer calculations, but the nonphysical temperature distribution would imply

that the user would be performing a heat transfer calculation on a non-existent temperature state in the central reflector. Should a user want to perform a heat-transfer calculation with perturbed thermal conductivity properties, implementing a fluence-dependency following the methodology in this paper would be beneficial, but the pseudo-temperature distribution to impose radiation-induced stresses would have to be excluded from the analysis. The fluence-dependent thermal expansion coefficient was also excluded from the model. This is because the pseudo-temperature distribution required a pseudo-thermal expansion coefficient to simulate radiation-induced stresses. The thermal expansion coefficient used in this analysis, then, did not match actual thermal expansion coefficient of IG-110 graphite, but was chosen instead to satisfy physical requirements for the irridation-induced stress model. The choice of this value is elaborated upon in section 3.4.

Lastly, the tensile strength of the material changes as a function of fast neutron fluence. This was not accounted for in the model as we aimed for a conservative estimate for the central reflector lifetime. The addition of fluence-dependent strength would add a factor of ~2 to the UTS of the material post-irradiation. By not accounting for this mechanism, the lifetime estimate will be shorter and also be more representative of the UTS of the entire component: the heavily irradiated edges and the low-fluence center.

3.2 The Pseudo-Temperature Distribution

Code packages such as COMSOL do not come readily equipped to perform a radiation-induced stress calculation, provided some fluence distribution in a reactor component. In projects like the HTGR and HTR-10, codes were developed in-house to analyze these types of stresses [5,19,28]. Throughout its lifetime, the inner central reflector will see a strain composed of a number of different sources [11]:

$$\epsilon_{tot} = \epsilon_{thermal} + \epsilon_{creep} + \epsilon_{radation} + \epsilon_{pressure} + \varepsilon_{other}$$

Because the strains are additive, they can be evaluated separately and compared to one another throughout the lifetime of the reflector. That said, they are not mutually exclusive, as radiation damage does influence material properties, and can influence the magnitude of strains not obviously attributed to radiation (such as thermal stresses). With this in mind, evaluating the stresses (or strains) of radiation-induced swelling was the primary objective, and other stresses could help determine the overall relative effect of radiation-induced swelling.

Graphite is a historically used reactor material, so a significant amount of data exists on the amount of swelling that will occur in a reactor environment. For radiation-induced swelling, measurements to specific types of NGG are available in the literature [24,27,31]. Below is the correlation for IG-110 that was used for this project, taken as a quadratic fit from the data for Fig 3.2.1.
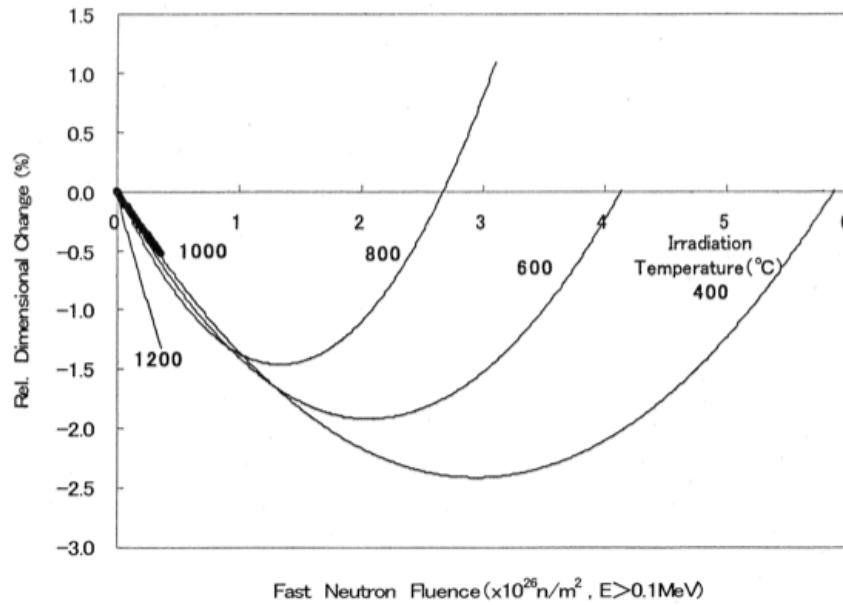
Figure 3.2.1: Dimensional Change of IG-110 Graphite at Various Irradiation Temperatures [31]

By fitting a curve to this data, a function for the dimensional change of graphite (strain) as a function of fluence can be determined from a quadratic fit, which would approximately resemble:

$$\epsilon_{radiation\ swelling} = xxx * \Phi^2 + xxx * \Phi + \Phi$$

where Φ is the reported fluence measured in 10^{22} n/cm², or 10^{26} n/m².

Knowing that for a particular fluence under zero stress an unrestrained strain is induced, it is then possible to think of other strain-inducing mechanisms that occur in nature. In particular, in extreme temperature environments, with high thermal gradients, one can observe significant thermally-induced strains. The end product of such a thermal environment and the radiation environment for this case is the same: a resultant strain that, under restrained conditions, induces stress. It is then possible to consider an alternative approach to simulate the radiation-induced stresses in COMSOL, where the user uses the thermal expansion physics to reflect radiation damage physics instead. Consider, for example, the equation for thermal stress:

$$\varepsilon_{thermal} = \alpha(T - T_{ref})$$

where α is the coefficient of linear thermal expansion (if the volumetric expansion coefficient is given, it must be converted to the linear expansion coefficient), and T_{ref} is the unstrained reference temperature. Consider also the strain resulting from radiation-induced swelling, which can be fit to the data with a polynomial equation:

$$\epsilon_{radiation\ swelling} = xxx * \Phi^2 + xxx * \Phi + \Phi$$

Consider, then, if one were to use a temperature distribution that gave the same strain:

$$\epsilon_{radiation\ swelling} = \epsilon_{thermal}$$

the radiation swelling can then be imposed with an arbitrarily chosen thermal expansion coefficient and temperature difference:

$$\varepsilon_{radiation\ swelling} = \alpha(T_{fluence} - T_0)$$

where T_0 is an arbitrarily chosen unstrained reference temperature, and alpha is an arbitrarily chosen thermal expansion coefficient. The thermal expansion coefficient can be any number, but the criteria used for the purpose of this study was limited by: ensuring that the quantity $T_{fluence}$-T_0 never got too 'extreme', such as a 10000K temperature difference, and also making sure that at the maximum contraction $T_{fluence}$ never could be below 0K—a nonphysical simulation. Rearranging, the above equation, and replacing:

$$T_{fluence} = \frac{\varepsilon_{radiation\ swelling}}{\alpha} + T_0$$
$$T_{fluence} = \frac{xxx * \Phi^2 + xxx * \Phi + \Phi}{\alpha} + T_0$$

Consequently we now have an equation for the fluence-dependent temperature profile in a reactor component. For this particular project, the correlation used (with fluence in terms of 10^{22} n/cm^2) was:

$$T_{fluence} = 229.9 * \Phi^2 - 617.4 * \Phi + 546.24$$

A temperature distribution can then be imposed in COMSOL or any other multiphysics package that reflects the distribution of radiation-induced swelling from the fluence profile within the central reflector. This will enable a more thorough analysis of the stress profiles that the component will see, and the limitations of this key component throughout its lifetime can be evaluated.

It is because there is a distribution of radiation damage within the reflector that this methodology is required. Should a key component be small enough that no gradient of fluence is imposed across the component, this calculation could be performed without the assistance of a finite element package such as COMSOL. The geometry of the central reflector is also limiting. In cases with simple geometry—a cylinder or sphere, for example—it is possible to calculate the stress distribution without the aid of a computer. Because a more complex geometry is anticipated in future iterations of the central reflector, it was necessary to develop a computational approach to this problem.

3.3 MCNP5

The MCNP5 model was constructed to reflect the same dimensional and material composition as the CAD model to be discussed in the subsequent section. The precise core configuration of the PB-FHR is described in previous publications [12], so this discussion will be limited to the central reflector and the basic core configuration.
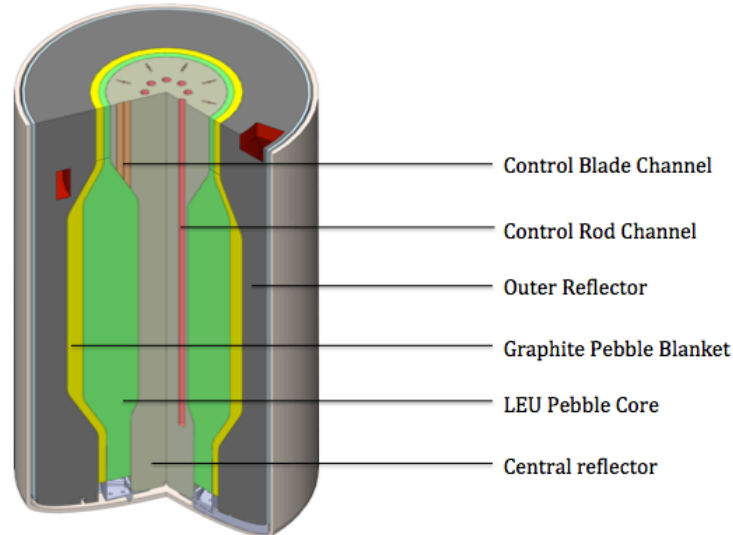
Figure 3.3.1: CAD Model Cutaway of PB-FHR Core

The fueled pebbles are represented in the above image by the green shaded region in the core. The pebbles enter the reactor core from the bottom and flow upwards through the core, as they are neutrally buoyant in the coolant, which moves upwards due to natural circulation. The pebbles surround the graphite central reflector, making this an annular core design. The central reflector houses the control rod channels, as well as guide channels for control blades that insert directly into the bed. The outer reflector is protected from a fast neutron flux by an inert graphite pebble blanket, displayed in yellow in the figure above. The inert graphite blanket also moves through the core as the fueled pebbles do, and so can be replaced during operation. The inner reflector cannot have an inert graphite pebble blanket as a shield, as the pebble blanket would have adverse effects on the reactivity worth of control rods, rendering them less effective for reactivity control.
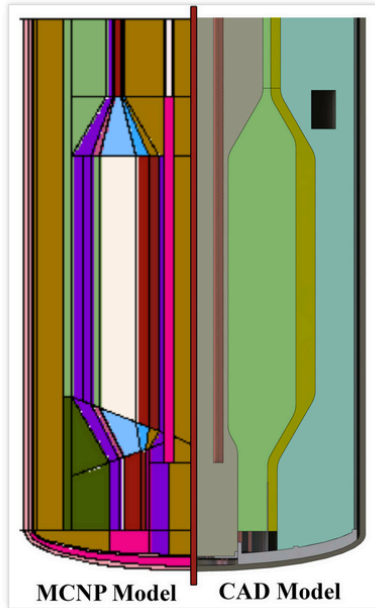
Figure 3.3.2: MCNP vs CAD model of PB-FHR Core, [12]

The MCNP model and the CAD model have been matched as closely as possible, but limitations between the two methods prevent them from being identical. To ensure that the results obtained from MCNP were placed in the correct locations on the CAD model, the results were scaled to the central reflector axial centerline, which is the region of the highest fast flux, and thus the region of highest importance. Below a central reflector specific image of the CAD rendered central reflector with regions and dimensions labeled can be found.
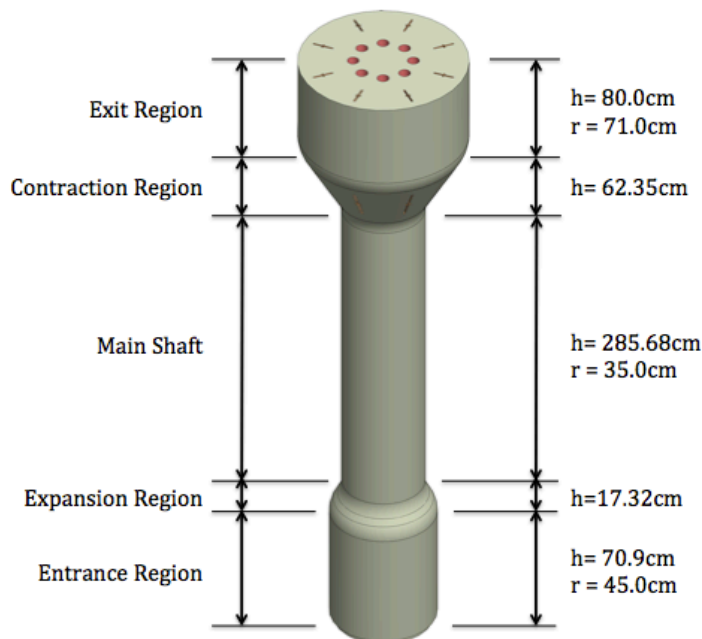
Figure 3.3.3: Relevant Central Reflector Dimensions and Labeled Axial Segmentation

The fuel composition of the MCNP5 model represents the equilibrium state, and was determined using the method detailed by Cisneros [12]. The equilibrium state of the core was used to determine the fast fluence, and thus the radiation-induced stresses, for a number of reasons: (1) the central reflector is likely to be in the core for several pebble lifetimes, and so will see an equilibrium core for the majority of its lifetime, and (2) a precise approach to equilibrium will be determined based on future analyses. Depending on the approach to equilibrium used, the neutron energy spectrum may vary, which would affect the dose rate differently in the inner central reflector. Performing an analysis that reflects the startup of the core would be contingent upon the evaluation and choice of a startup method, and so cannot be done at this time. Additionally, a detailed, time-varying analysis of the core—including the aforementioned startup and approach to equilibrium—would only be necessary after the PB-FHR can be considered a viable reactor concept, as it will involve a significant investment in computational resources and methods development. This analysis is one aspect of the proof of viability, and so will inform the choice whether to pursue those analyses.

With the geometry of the PB-FHR defined from previous studies, MCNP5 [6] was used to determine the fast fluence distribution in the graphite central reflector. This was done with a series of F4 mesh tallies. A sample of one of these mesh tallies is shown below.

Figure 3.3.4: Example Mesh Tally Used to Tally Fast Flux In Central Reflector

The first line geom = cyl denotes the mesh tally's coordinate system to be cylindrical. Emesh specifies the energy meshing that the user wishes to bin. The first bin is from 1e-11 MeV to 0.1MeV, and the second bin is from 0.1 MeV to 20 MeV. Recall that the literature values for the radiation-induced swelling was measured in terms of the fast fluence, where the fast fluence was specified to be all neutrons with an energy greater than 0.1 MeV. The three intermediate lines specify the geometry of the mesh tally for the i j and k coordinates, respectively. Here i represents the radial coordinate, j represents the axial coordinate, and k is the azimuthal coordinate. The first line, imesh specifies two intervals of mesh, the first from 0.0 to 50.0cm with 10 bins in that interval and the second from 50.0cm to 71.0cm with 10 bins in that interval. Each interval can have different amounts of bins, which is exemplified in the proceeding line in jmesh. Note that this is only one of the tallies used for this calculation. Each axial region in Fig 3.3.3 had a separate mesh tally. The most important region of the central reflector, the main shaft, has a much finer meshing with 0.5cm radial zoning in the outer 10cm of the shaft.

The f4 binning of fast flux could have been done with a single f4 mesh tally running the entire length and width of the central reflector, however it would not be an efficient way to obtain results. The edges of the central reflector see the highest

fast flux, and so are very important for stress analysis. The inner portions see a much softer energy spectrum, and so will not be as affected by the fast flux. Thus the edges of the central reflector require a finer meshing, but at some axial locations the edge of the reflector lies at a different radius than others. Performing this calculation with a single mesh tally would require a fine mesh over areas of the central reflector with low fast fluence, and to achieve statistical significance in the results, the calculation would take much longer. As a result, five different mesh tallies formed a composite overall meshing of the central reflector, with each mesh tally segmenting axial regions of the central reflector: the entrance region, the diverging region, the main shaft, the converging region, and the exit region.

The results from the f4 tally are units of neutrons/cm^2-source neutron, which is a time independent result. In particular, an f4 mesh tally is defaulted to the track-length estimate of the flux, averaged over the mesh cell [6]. To obtain a flux, this quantity must be scaled to the source neutron emission rate. By using the total thermal power of the core, the energy per fission, and neutrons emitted per fission[1], the source neutron emission rate was calculated[2]. Multiplying the result of the f4 mesh tally and the calculated source neutron emission rate, the flux in each mesh cell volume was calculated (units of neutrons/cm^2-second). The fluence in each mesh cell volume was then calculated by multiplying flux by the time of irradiation, returning units in neutrons/cm^2.

Each calculated fluence corresponded to a geometric volume that was defined in the mesh tally previously. To import this into COMSOL, every fluence value was assigned to a corresponding data point at the center of each mesh cell. Then COMSOL read each fluence value at the R,Z midpoint location and interpolated linearly to the next mesh location. The plotted fluence distribution on the COMSOL volume is displayed in Fig 3.3.5. Additionally, the fluence distribution at a 275cm cut plane is displayed in Fig 3.3.6.

It is of importance to note the very different mesh cell size between 0-0.25 cm and 0.25 to 0.35m in fig 3.3.6. This is due to the differing mesh cell size in MCNP, which was limited by computational time and statistics. This inner mesh was not refined to a further extent because the region is less important than the higher fluence rate outer region of the central shaft, which dominated the limiting tensile loading in the central reflector. Therefore a coarser mesh to see the trend of fluence distribution sufficed for this inner region. While this fluence data is taken from COMSOL, it reflects directly what was outputted from MCNP5. However, COMSOL does interpolate between values taken from the coarser MCNP5 mesh to reflect the mesh that COMSOL will use to perform the stress analysis. Therefore the data in Figure 3.3.6 represents the flux that COMSOL is using to perform the stress analysis, which was taken (and interpolated) from MCNP5. The fluence data for 0.25 to 0.35m had errors of less than 1%.

---

[1] 236 MWth was used as the nominal thermal power of the PB-FHR core, 200 MeV per fission was used for the energy per fission, and 2.564 as the value for neutrons emitted per fission.

[2] The resultant source neutron emission rate was 1.88e19 source neutrons/second.

Fluence (10^22 n/cm^2) at 2 Effective Full Power Years

▲ 0.586

0.5

0.4

0.3

0.2

0.1

▼ 4.6038×10⁻⁵
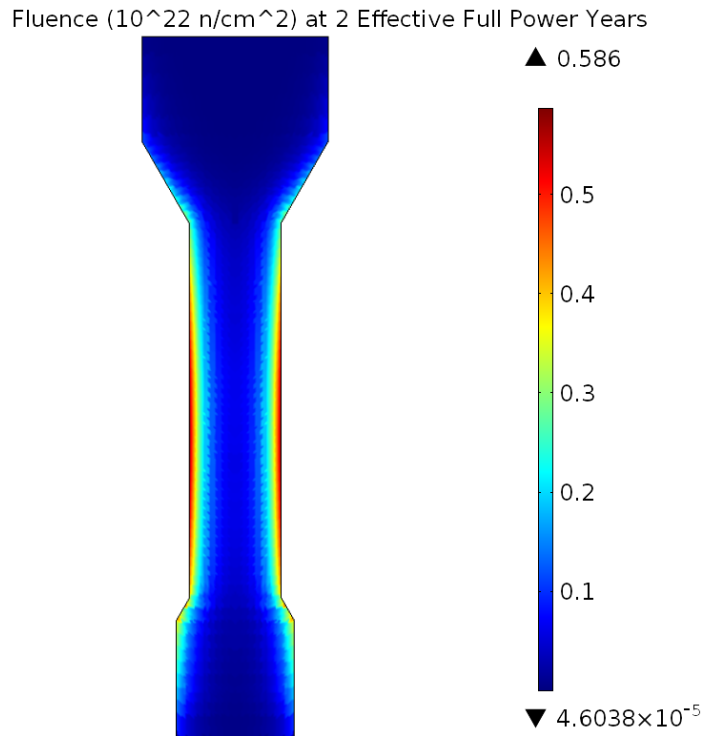
Figure 3.3.5: Fluence Distribution in the Central Reflector After 2 Effective Full Power Years. Model Maximum and Minimum Values are Labeled on Extreme Ends of Colorbar Legend.

Central Reflector Fluence at Z = 275cm at 2 EFPY
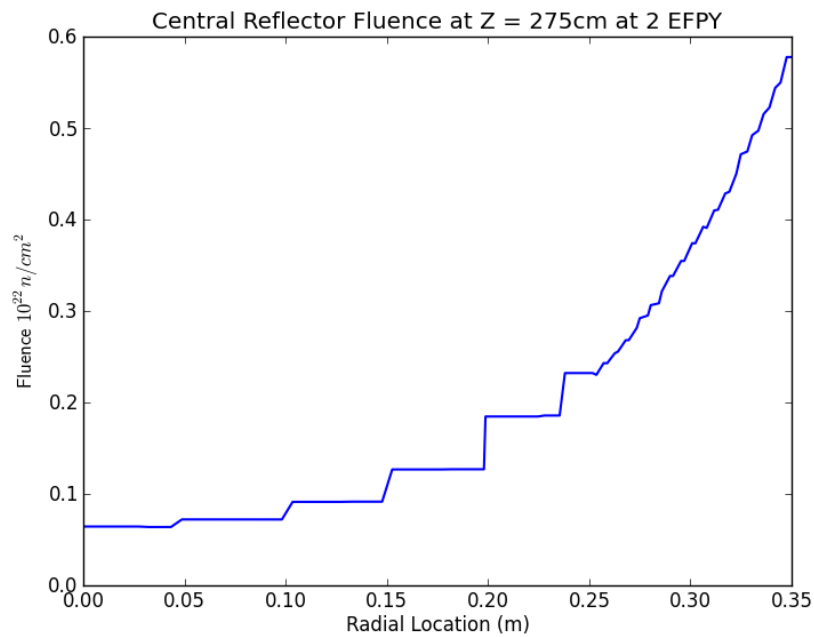
Figure 3.3.6: Fluence Data for Central Reflector Cutplane at Axial Midplane of Central Reflector. Fluence Units in 10^{22} n/cm².

3.4 COMSOL

As previously mentioned, the structural mechanics module was used in COMSOL [13] to perform the stress analysis. The core geometry was readily imported into COMSOL using previous CAD drawings done in SolidWorks detailed in previous publications [21,22]. The COMSOL model used 2-D axisymmetric geometry, as the central reflector has azimuthal symmetry without control rod channels. However, in future iterations with control rod channels and added complexity to the central reflector structure, a model using 3D cylindrical geometry will be required. COMSOL has a multitude of physics package extensions available to the user, but the structural mechanics and heat transfer modules were the two primarily utilized for this project. In the anticipation of a continuation of this work, this section will attempt to step through the creation of the COMSOL model used for this project.

First the geometry was imported with the CAD import module as exemplified in Fig 3.4.1a and 3.4.1b.
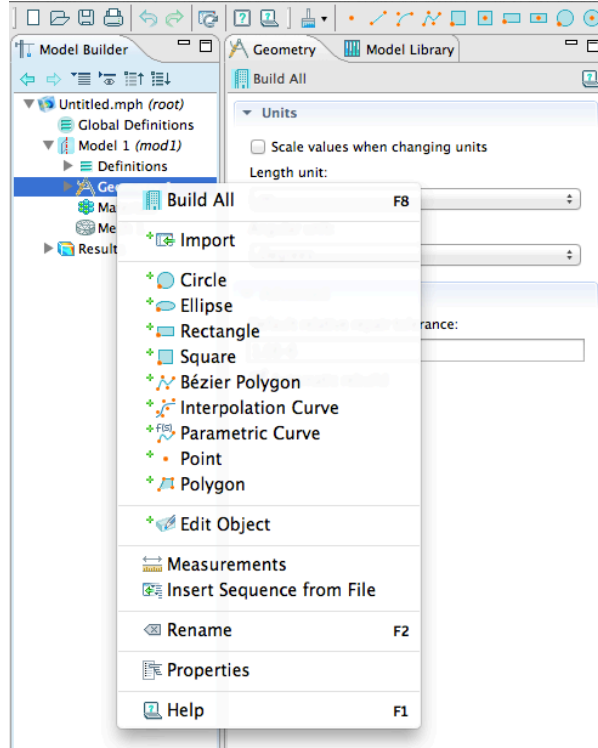
Figure 3.4.1a: Adding the Import Module to Import Geometry to a COMSOL model
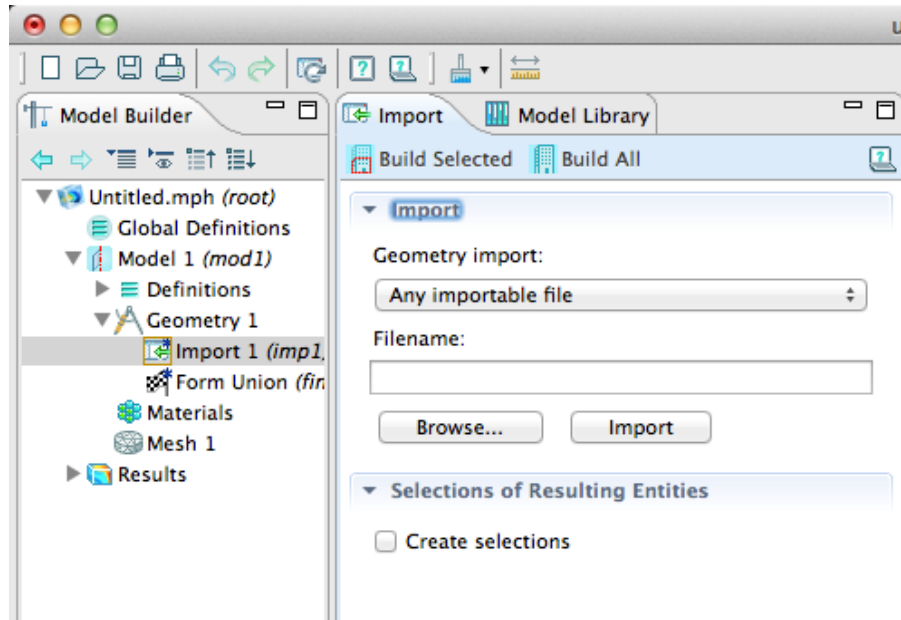
Figure 3.4.1b: Browse appropriate files for CAD model to import

The user then needs to add the appropriate physics packages to the model (Fig 4.3.2a). In this case, the solid mechanics module is chosen (Fig 4.3.2b). However, multiple modules can be used so long as the user defines variables adequately for a solution to be found.
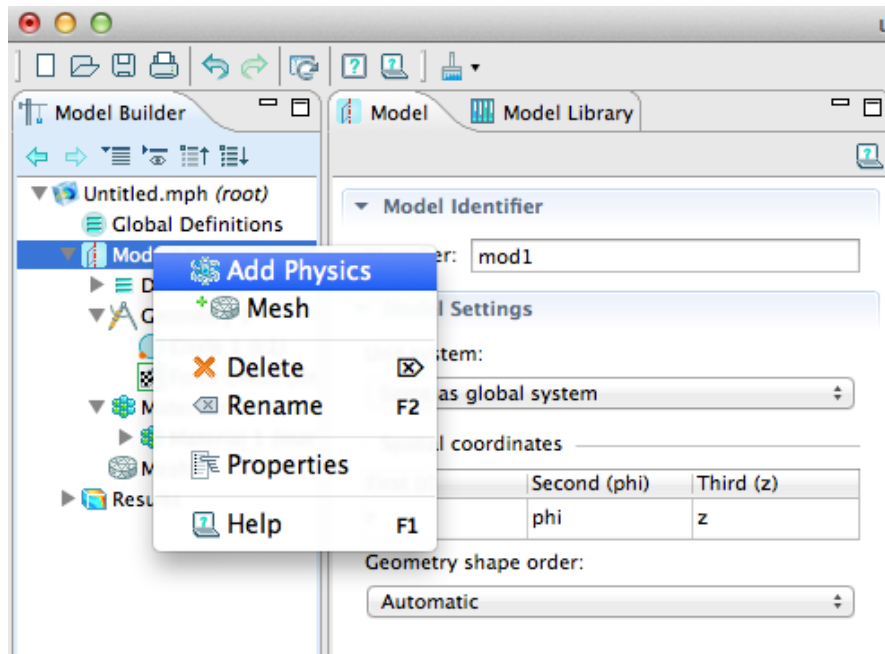
Figure 3.4.2a: Add Physics to COMSOL Model
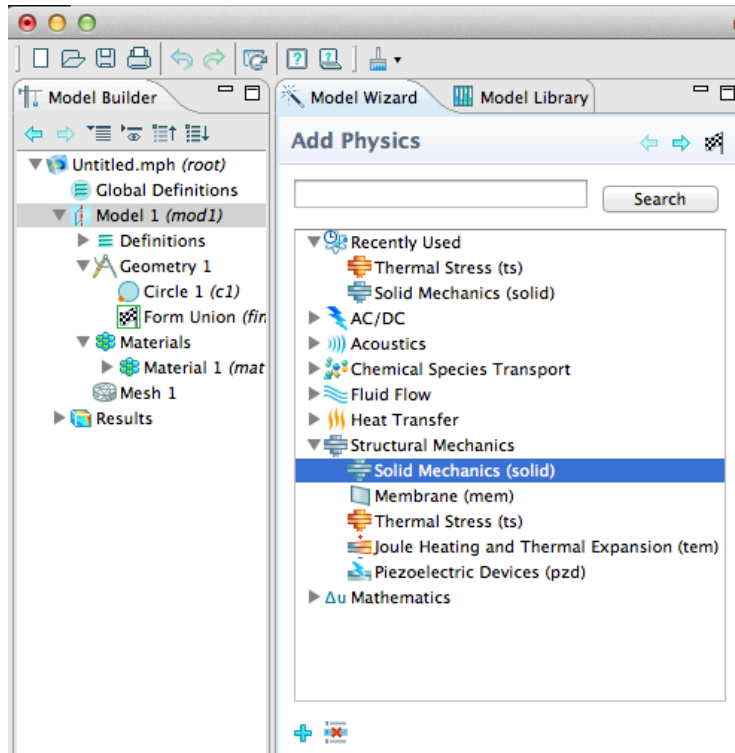
Figure 3.4.2b: Available Physics Modules for Simulation. In this study, solid mechanics was used (refer to 3.4.9 for how to add thermal expansion to this module).

       With the geometry imported and the module choice finalized, one can begin with defining the variables and parameters required for the calculation. In the immediate proceeding paragraphs, this paper will attempt to step through the pertinent portions of the model for calculating radiation-induced stress so future users can easily replicate this work.

       First, this model specifically used several fluence-dependent properties. In the global definitions drop-down menu, the functions that correlate various material properties with fluence are defined. Interpolation 1 in the figure below interpolated the fluence data and the data from MCNP5.
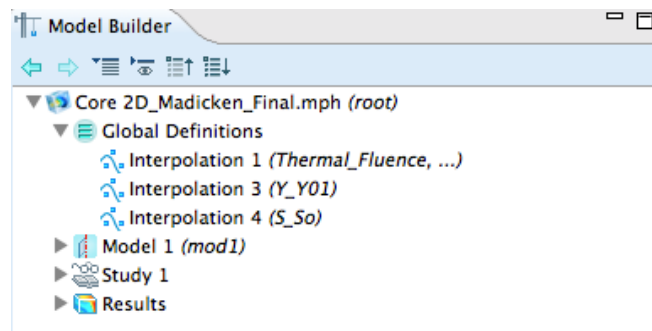
Figure 3.4.3: Global Definitions

Expanding this tab, one can see Interpolation 1 has four different data sets each with the same two independent variables. Data set 1 is the "Thermal Fluence", Data set 2 is the "Fast Fluence", Data Set 3 is the "Total Fluence" and Data Set 4 is the "DPA". All four data sets are imported from a document entitled Import1yr.csv. The "position in file" corresponds to what column they lie in in the .csv file. Because these data sets correspond to various axial and radial positions of the central reflector, the two independent variables are the radius, R, and the axial height, Z, which are given in arguments of cm.
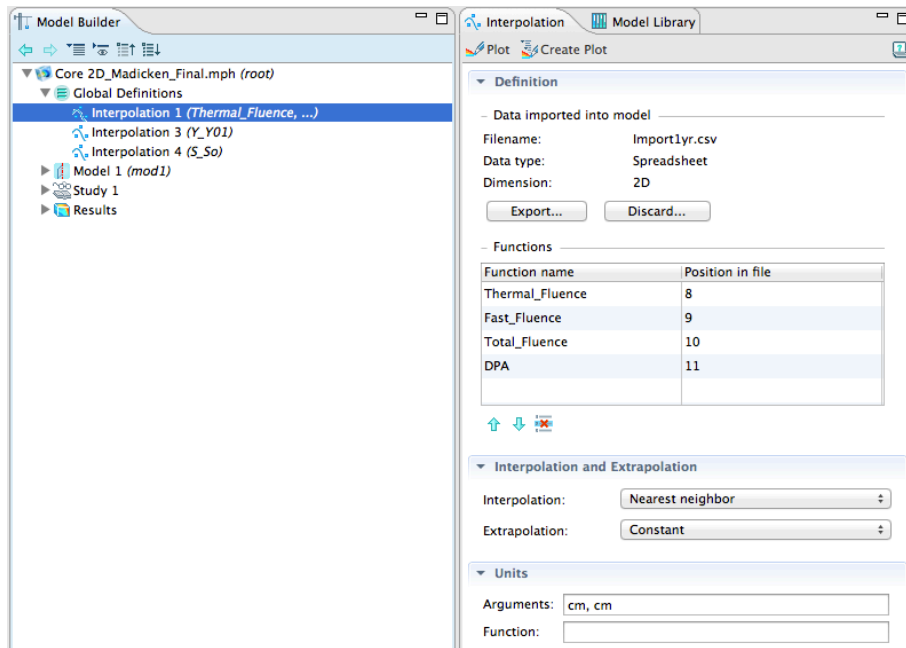
Figure 3.4.4: Globally Defined Data for COMSOL Model Applications.

If either the Interpolation 3 (Y_Y01) or Interpolation 4 (S_So) tab is expanded, one can see that the data is directly inputted into the COMSOL model, rather than being imported from a .csv file. The function depends on t, which is, in this case, the fast fluence, and outputs the relative change in the young's modulus (giving Y_Y01(t))or the strength change (S_So(t)) in the material. The interpolation type chosen for all of these global definitions was nearest neighbor interpolation, as not enough information exists on the behavior of these functions to warrant a polynomial interpolation or higher order fit.
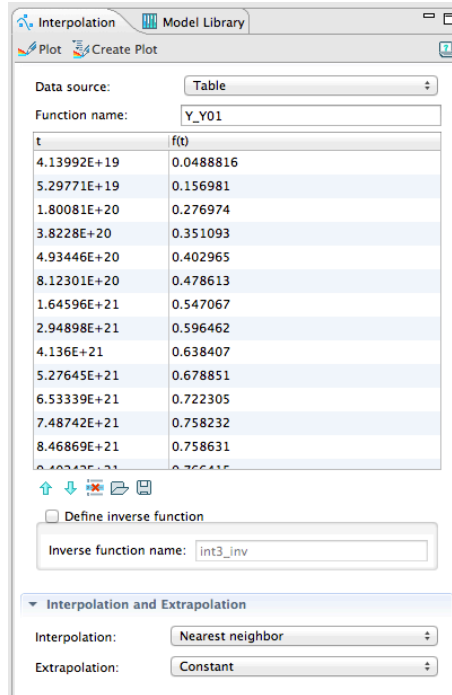
Figure 3.4.5: Imported Data for Interpolation

The global definitions define how young's modulus, the strength, and the fluence vary with r and z. However, the model-dependent variables are in the drop-down menu inside Model→Definitions→Variables.
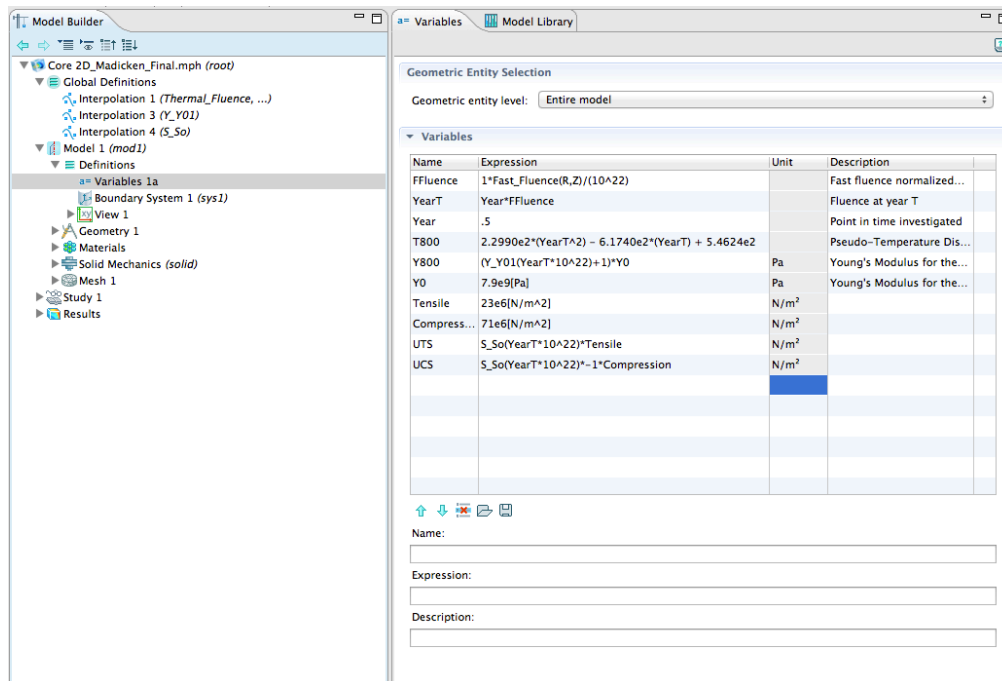
Figure 3.4.4: Model-Specific Variables

FFluence normalizes the Fast_Fluence value from the global definition Interpolation 1 to 10^{22} n/cm². The "units" in this fluence are not strictly a fluence, as

they have been normalized to fluence per year. YearT takes the FFluence value and projects it in time, which is a function of the variable "Year", outputting units of fluence at year T. This is valid because the fluence value will increase in a differential volume linearly with time. However, should the fast fluence vary as a function of time—due to spectral shifts during the core's lifetime, for example—this particular treatment of the fast fluence would require modification. The variable "Year" can be changed by the user to perform a stress analysis at a particular point in the reactor's lifetime. Because the purpose of this study is to determine the lifetime of the central reflector, this variable is extremely important.

T800 takes the 800K line for dimensional change in Figure 3.4.4 and returns the pseudo-temperature distribution as a function of YearT with the method expanded upon in section 3.2. It is the function that takes a fluence as an input and outputs a temperature value. This is the most important function in this section, because it transforms the spatially fluctuating fluence to a spatially distributed temperature. Y800 does the same, but instead uses Interpolation3 to determine the change in young's modulus as a function of the total fluence. UTS and UCS also use the correlation from Interpolation 4 to determine the change in strength of the material as a function of fluence. Y0, Tensile, and Compressive are the unirradiated values for the young's modulus, the tensile strength and compressive strength of the material. Note that these are both material properties of the material, but are not required to perform any of the stress analysis calculations in this model, so they have been included in the "Variables" section.

If, instead, the properties were required for the stress analysis calculation, they would be defined in the Model→Materials→IG-110 drop down tab. The variables with green check marks are "required" to performing requested calculations, and so this particular model can be solved because all variables are defined properly.
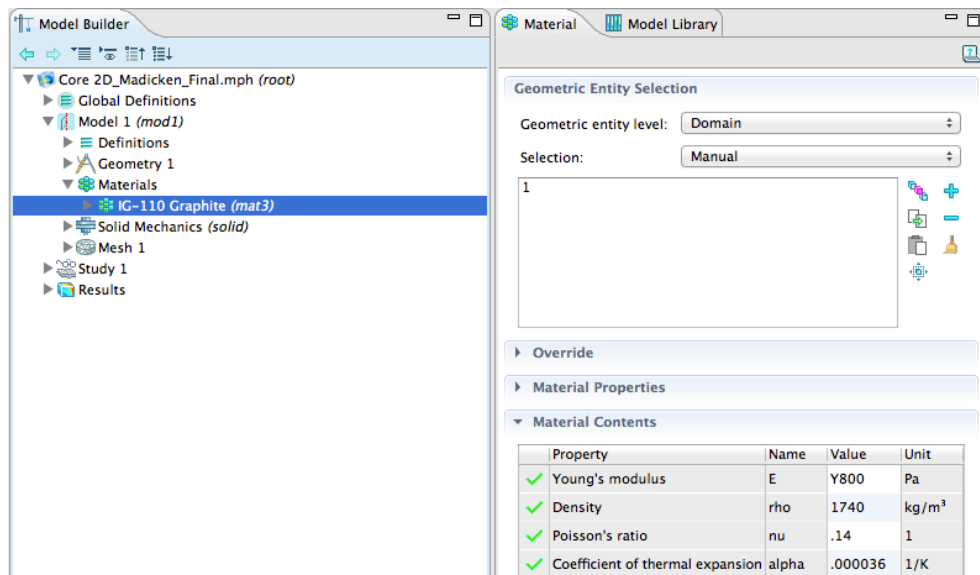
Figure 3.4.5: Material Properties Specification

Note that all of the material properties are listed as numbers, with the exception of Young's modulus, which calls to Y800, calculated and defined in the Model→Definitions→Variables tab. This is becauseY800 is a fluence-dependent material property, but all other material properties are assumed to remain constant with time. Unless significant mass loss occurs in the graphite, density should remain relatively constant with time. Because radiation creep is not being simulated in this particular analysis, it is assumed that poisson's ratio will remain constant. It should be noted that poisson's ratio does not remain constant with time under irradiation conditions, but its changes are accounted for in radiation-induced creep. Radiation-induced creep was not in the scope of work for this study, so it was not incorporated. All non fluence-dependent material properties in this tab were chosen to match the IG-110 values acquired from the literature, summarized in section 3.1.

Up to this point, the model variables and material properties have been defined, but the defined parameters have not been projected onto the model geometry. This is done in the solid mechanics tab.
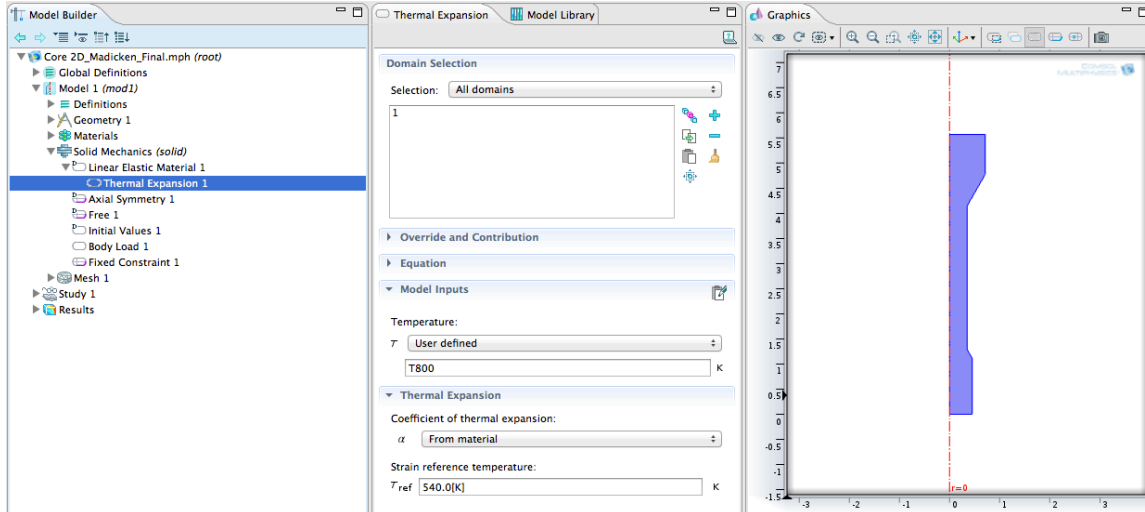
Figure 3.4.6: Definitions in the Solid Mechanics Physics Package

Under the solid mechanics module tab, several objects are listed. The body load is the condition that puts the material in space under a gravity load. The Axial Symmetry definition chooses a surface to rotate the shape about. In this case, it is the centerline. "Free1" selects the surfaces that are free to expand in space. Because the central reflector is in a gravity load, the top and outer edges are selected. Conversely, "Fixed Constraint 1" notes which surfaces cannot freely expand in space, which is the bottoms surface. "Initial Values 1" defines no important parameters, but was automatically included with the Solid Mechanics module selection. The icon to the left of each item's description denotes what type of variable the item is. A purple edge indicates that a surface must be selected, while a white oval indicates that the item is a volume selection.
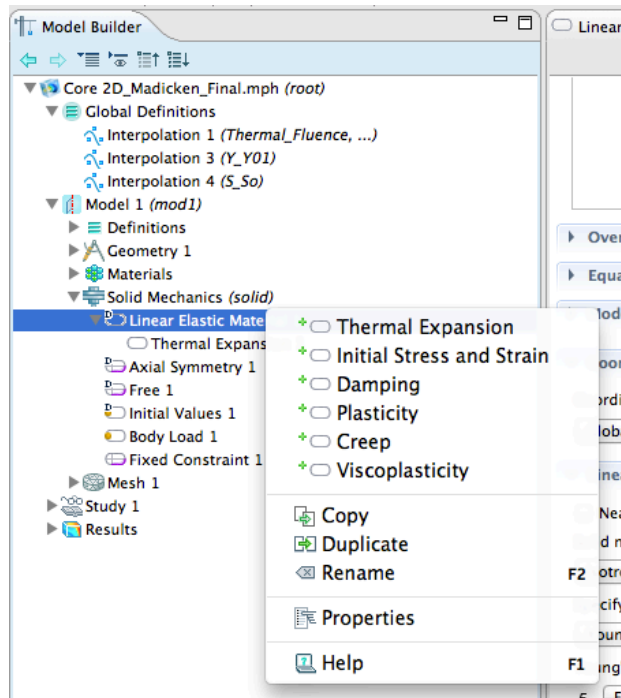
Figure 3.4.7: Adding Thermal Expansion to the Solid Mechanics Physics Module for the Simulation.

The Linear Elastic Material item has an expansion option, which in this case has been to include thermal expansion. As elaborated upon in section 3.2, thermal expansion in this project is used to "simulate" radiation-induced expansion. By right clicking on the Linear Elastic Material, a number of alternate physics options can also be chosen for the simulation.

Looking in the "Thermal Expansion 1" tab to the right of the Model Builder, one can see that this is the location where the temperature distribution is finally imposed on the volume. Under the "Model Inputs" tab, the temperature is user defined, and T800 has been entered. Recall from the previous paragraphs that T800 is the calculated temperature distribution that correlates to the fluence distribution over the volume. T_{ref} in the thermal expansion tab is the unstrained reference temperature. Here it has been chosen to be 540K. Like the thermal expansion coefficient, this number is arbitrarily chosen by the user. Here it was chosen with the criteria that at maximum contraction, the material's pseudo-temperature could never go below 0K. If the user chooses a different thermal expansion coefficient, a different T_{ref} could also be chosen for the simulation.

To run the simulation, the user must right-click on the study tab, and click compute. Depending on the calculations that the user would like to be performed, this can take from a few seconds to a few minutes. By adding different plot groups to the results tab, the user will need to rerun the computation accordingly.
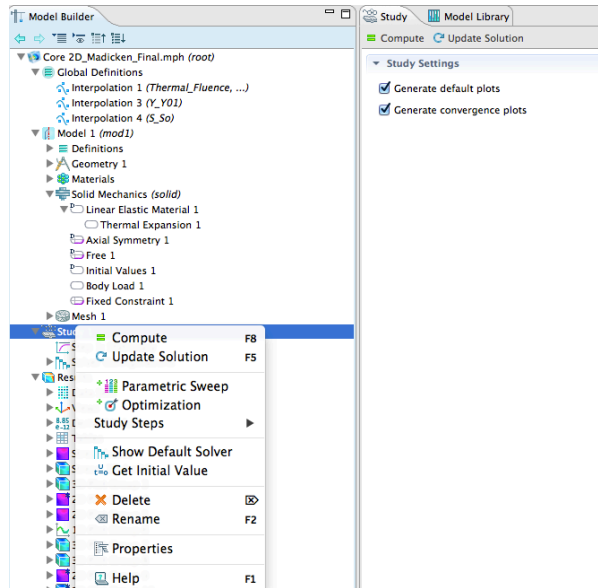
Figure 3.4.8: Executing the COMSOL simulation. Compute will recomputed all numbers, which is required if any of the variables mentioned in earlier figures are changed.

As a sanity check, one should expect that at early-life fluences that the pseudo-temperature distribution should first trend towards cooler temperatures, and then at higher fluences trend towards hotter temperatures. Earlier the "Year" variable was specified at .5, indicating that the central reflector has been irradiated for 6 months. This is early in the irradiation period, so the outermost edges of the central reflector should be lower in temperature than the unstrained reference temperature, T_{ref}. Plotting the temperature distribution at a cut plane halfway up the central reflector, it is evident that the center of the central reflector has relatively little temperature perturbation (and, consequently, has seen very little fast fluence), and the edges are "cooler", as shown in Fig 3.4.11
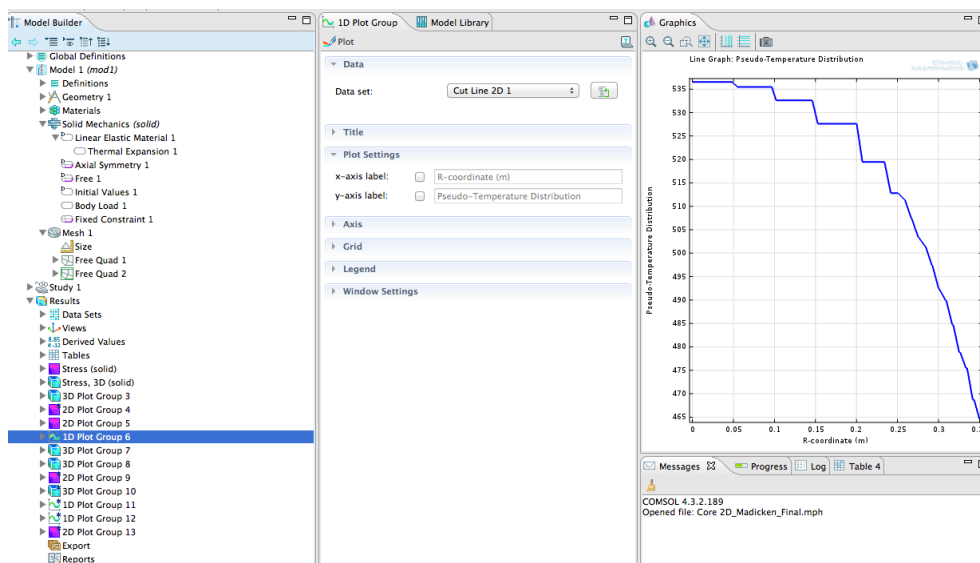
Figure 3.4.9: Plotting Temperature at a cut plane with COMSOL

The user is free to explore the plethora of options that one may choose to plot in the results section. However, it is outside the scope of this paper to describe in detail each of these options, so the author leaves it up to the reader for this exploration.

3.5 Failure Criterion:

An important limitation for any reactor component is its time to failure. Because the central reflector is a key component for safety and stability of the reactor system, it is essential to determine how long it will last in the core. A common rule of thumb used for graphite component lifetime evaluations is the "turnaround point". However, this is a rather arbitrary rule, and one can imagine several scenarios where a component might be at the "turnaround point". Is it when a small segment of the component reaches the turnaround point? What defines "small"? How small could a segment be? How different is the lifetime estimate if one considers the average fluence seen by the component? It is evident that a more rigorous approach to evaluating the lifetime is required for large components of critical importance to the reactor system. Should this study provide the same result as the "turnaround point" rule, then any confidence in the applicability of this rule for this system can be justified.

The next iteration of failure, then, is to determine at which point the graphite will exceed its material limitations: the ultimate tensile strength or the ultimate compressive stress. Because the central reflector is in a static load, we will neither consider the bending strength nor the twisting strength. For this study, the ultimate tensile strength was chosen. It has been shown that materials can withstand conditions beyond their compressive stress, but beyond the UTS will result in significant cracking and crack propagation. Additionally, the UTS is a lower total stress (Table 3.1.1) and so will be more limiting. Additionally, the central reflector will not see an environment where bending moments, twisting moments, or other similar situations in normal operation. These would occur in beyond design basis events (BDBEs), and so the lifetime of the reflector will not take into account these limitations.

Tensile and Compressive stress limits are determined by applying a load on a single axis of a sample. However, stresses in real systems are often multidirectional. The Von Mises criterion[11] is used in the latter cases. It can be summarized as a method to determine the overall stress in a differential volume, which is a sum of the root mean square of the principal stresses:

$$\sigma_{Mises} = \sqrt{\left(\frac{1}{2}\right)\left[(\sigma_x - \sigma_y)^2 + (\sigma_y - \sigma_z)^2 + (\sigma_z - \sigma_x)^2\right]}$$

The time at which the material's Von Mises stress exceeds the UTS is the absolute maximum amount of time at which it can be in the radiation environment. However, the actual lifetime of the component will realistically be when portions of

the central reflector reach some fraction of the UTS; when an engineering safety factor is incorporated. For the purposes of this study, lifetime evaluations were done for the point at which the central reflector reached the UTS, and did not include a safety factor. It should be emphasized here that the purpose of this study is for scoping and giving a point of reference for central reflector design. For design optimization for the central reflector and in future iterations of the reflector design, an engineering factor should undoubtedly be incorporated.

4. Analysis of The Solid Graphite Central Reflector

After the MCNP5 fluence distribution with sufficient statistics was obtained and ported to a COMSOL model with the aforementioned specifications, stress distributions at various stages in the core lifetime could be obtained. A substantial amount of data can be acquired from each of these time steps, so a snapshot at t=2 years (Figs 4.2-4.9) will be described in full here. Results for other time steps are available upon request from the author.

As a point of reference, the reflector loading at t=0 (Fig 4.1) is the unirradiated stress loading of the central reflector. For this particular analysis, a buoyant load was applied, as if the central reflector were placed in a bath of flibe at the average temperature of the coolant (650C). As indicated in previous sections, the ultimate tensile strength of IG-110 graphite is 25MPa. Also recall that the Von Mises stress is an indication of the tensile stress a macrobody loaded in three dimensions will experience. As such, the axis of the colorbar ranges from 0 MPa to just over 25 MPa, where any red coloring indicates that the component is beyond the ultimate strength. COMSOL defaults to showing the lowest and the highest data points' values on the extreme ends of the colorbar legend. It is evident from the coloring and the loading that the central reflector is well below its ultimate stress loading, and reaches a local maximum at the rigid boundary at the top. Important regions of the central reflector, like the axial midplane, are well below an MPa of loading.

At t=2 years, the Von Mises loading (Fig 4.2) has changed significantly. The maximum Von Mises stress seen by the central reflector is just over 130 MPa. The entire surface of the central reflector in the active region of the core has exceeded its ultimate tensile strength. It does not appear that a solid central reflector of this design will last even 2 effective full power years in the core, so some design modification will be necessary to make a central reflector of this type last longer in the core. It is not immediately evident from the figure below, but the maximum tensile stress (noted at the extreme end of the colorbar legend) is located at the corners where the central shaft meets the expansion and contraction portions of the central reflector. Note again that this t=2 years cut plane is a sampling of the several timesteps analyzed.
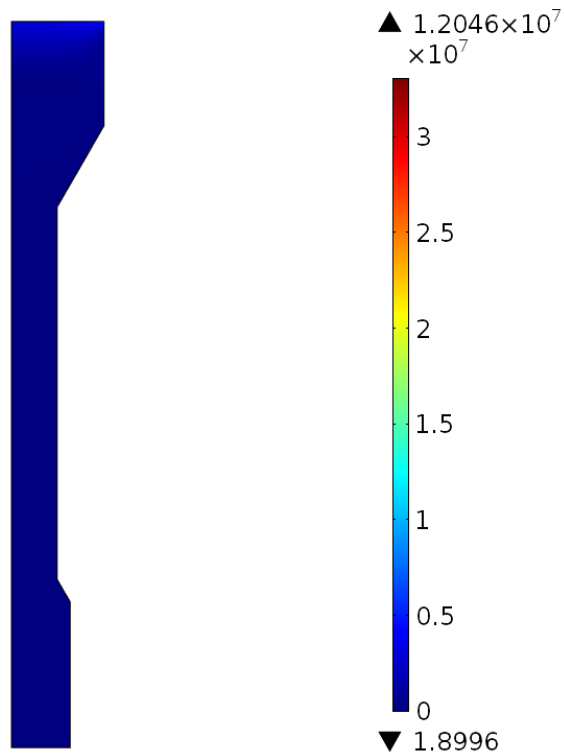
Figure 4.1: Von Mises Stress of Central Reflector Pre-Irradiation. Model Maximum and Minimum Stress Values are Labeled at Extreme Ends of Colorbar Legend.

As discussed in previous sections, the turnaround point was a time-limiting metric for reactor components of this type. The pseudo-temperature distribution can be used to find the turnaround point of this component. If the reflector temperature distribution reaches its original unstrained reference temperature (540K), then the reflector has reached the turnaround point. At the axial midplane (where the flux will be the highest, and so the turnaround point will be reached earlier in the components lifetime), the outer edges of the central reflector are still "cooling", reaching a low temperature of 263.4K (Fig 4.3). As such, it has not even reached the point of maximum contraction, and is well below the time at which it will reach the turnaround point. Therefore the turnaround point metric will tend to overestimate the central reflectors lifetime, and is not suitable for a large component of this type. A further exploration of this assertion is explored later in this section.

Von Mises Stress (N/m^2) at t = 2 years
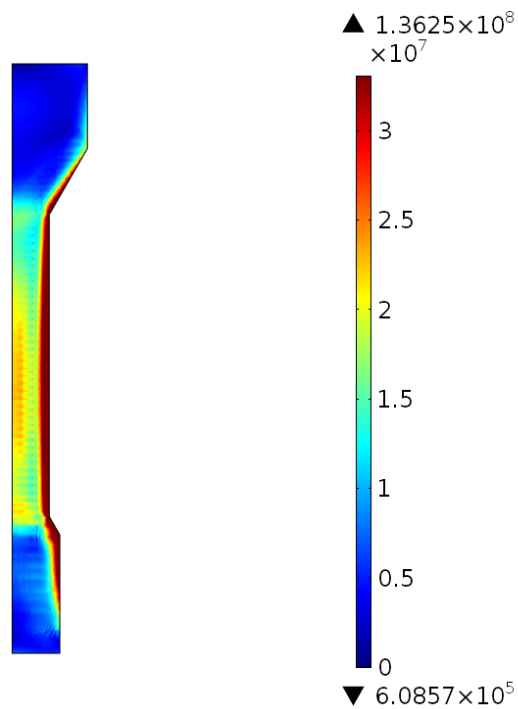
Figure 4.2: Characteristic Von Mises Stress for Cut Plane of Central Reflector After Two Effective Full Power Years. Model Maximum and Minimum Stress Values are Labeled at Extreme Ends of Colorbar Legend.

Pseudo-Temperature Distribution in Central Reflector (K) at t = 2 years
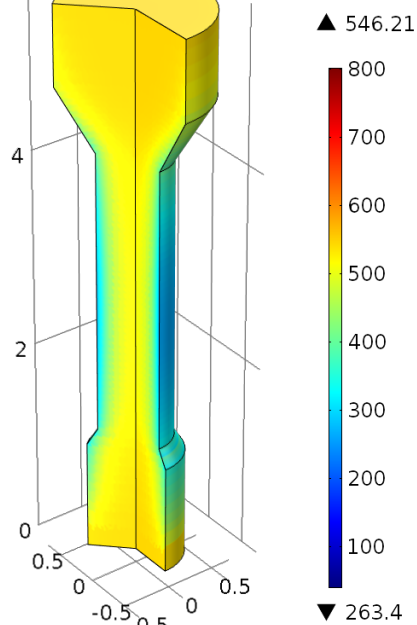
Figure 4.3: Characteristic Pseudo Temperature Distribution for the Central Reflector at 2 Effective Full Power Years. Model Maximum and Minimum Temperature Values are Labeled at Extreme Ends of Colorbar Legend. T$_{ref}$ is 540K.

The Von Mises stress is a sum of the squares of each of the resolved stress dimensional coordinates in space. Resolving each component of the stress reveals not only which stresses dominate the Von Mises stress, but also help to inform future design iterations. Note that these axes range from -7.1*10^7 to 2.5 *10^7 Pa, which are the UCS and UTS, respectively.

The stress tensor in r exhibits compressive behavior. The outer regions have contracted from shrinkage, adding a pressure stress on the inner region of the reflector, which has seen relatively little fluence, comparatively. Note that the UTS is exceeded only slightly (as noted on the upper end of the colorbar legend), at what appears to be the contraction and expansion regions, while the UCS is not exceeded at all.
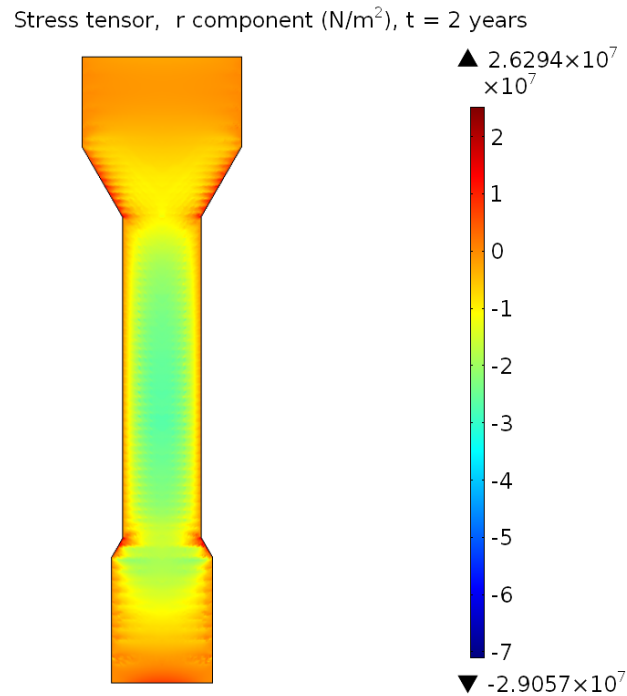
Figure 4.4: R stress component for XZ cut plane

The z component of stress has enormous tensile stresses. The shrinkage of the central region elements has created large tensile stresses farther up and down the central reflector shaft. As a result, this also creates a pressure stress on the shielded core of the reflector. This component of the stress has by far the largest range in stress and also exceeds the UTS by the greatest amount.

Stress tensor, z component (N/m^2), t = 2 years

▲ 1.3364×10^8
×10^7

2
1
0
-1
-2
-3
-4
-5
-6
-7

▼ -5.016×10^7
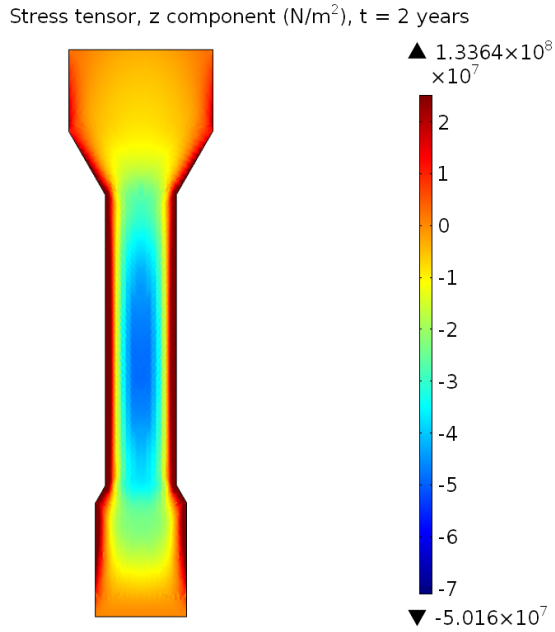
Figure 4.5: Z stress component for XZ cut plane

The phi component (or hoop stress) of the stress also exceeds the UTS, but not by as much as the z component of stress. However, the UTS is exceeded farther radially into the central reflector material. Both the azimuthal and axial stresses dominate the Von Mises stress, and will be the limiting factors in determining a lifetime estimate for the central reflector region.

Stress tensor, phi component (N/m^2), t = 2 years

▲ 8.1618×10^7
×10^7

2
1
0
-1
-2
-3
-4
-5
-6
-7

▼ -2.7451×10^7
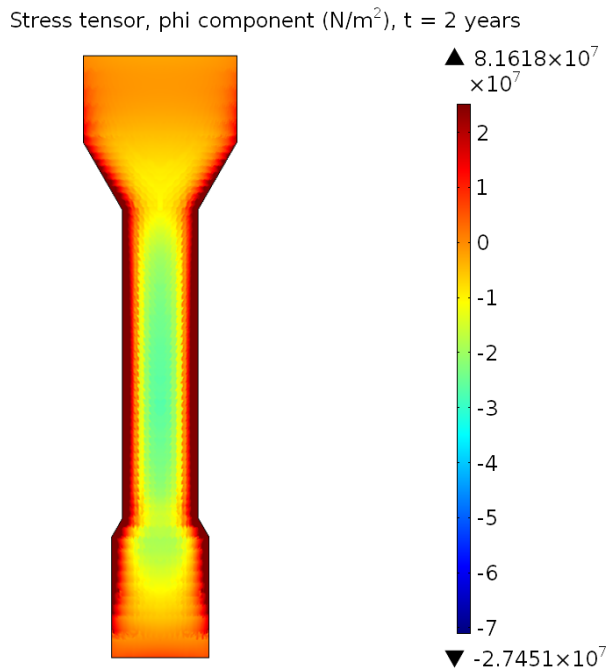
Figure 4.6: Phi stress component for XZ cut plane

While the vertical cuts of the central reflector reveals the stress distribution over the entire central reflector, a cut at the axial midplane (z = 275cm) of the

reflector will more readily reveal information in the highest fluence-rate region of the central reflector while not including the stress-concentrating corners where the converging and expansion regions begin and end, respectively. Figures 4.7-4.9 include the resolved stresses in R, Z and Phi plotted on this cutaway plane. The extreme ends of the colorbars on each figure reveal that, indeed, the peak tensile and compressive stresses on the XZ cutplane (Figs 4.4-4.6) are different than at the XY cutplane at z=275cm. In particular, both the Z and Phi components of stress have comparable maximum tensile stresses, but the phi component does not reach as great of a compressive stress. While the tensile stress is more limiting, a larger gradient of the stress over a linear distance will add to the Von Mises stress and tend towards shortening the lifetime of the central reflector.
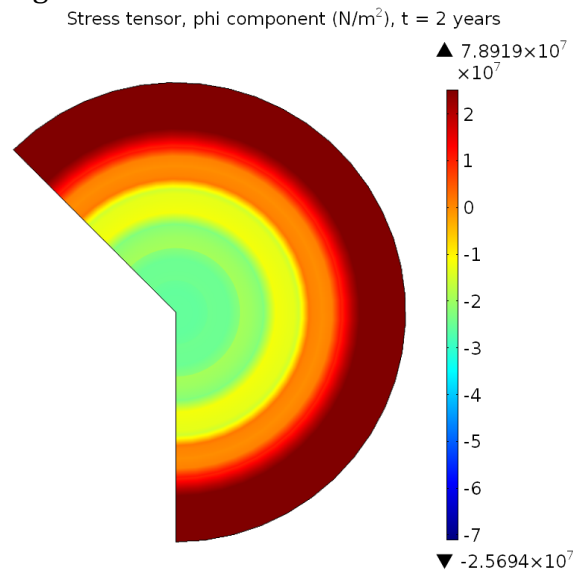
Figure 4.7: Phi stress component for cut plane at z = 275cm
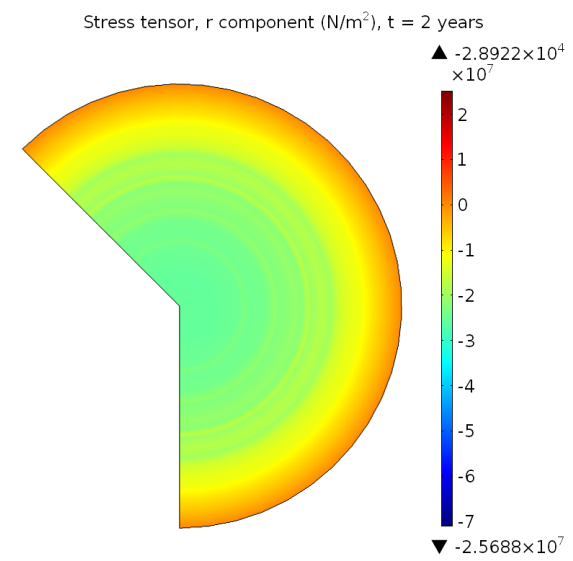
Figure 4.8: r stress component for cut plane at z = 275cm
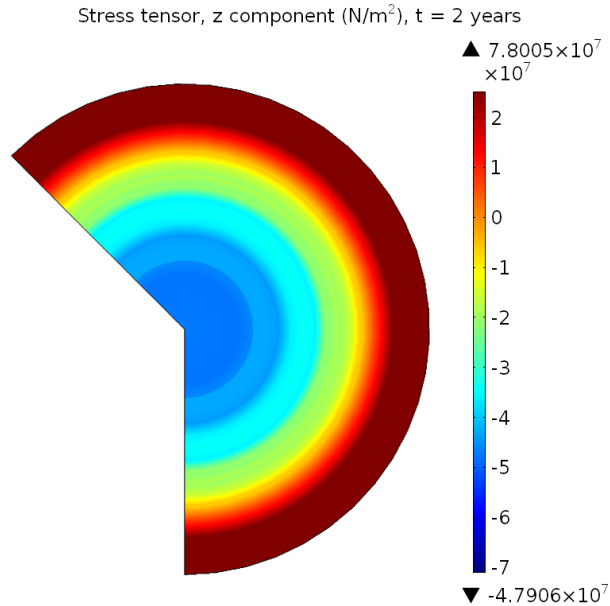
Figure 4.9: Z stress component for cut plane at z = 275cm
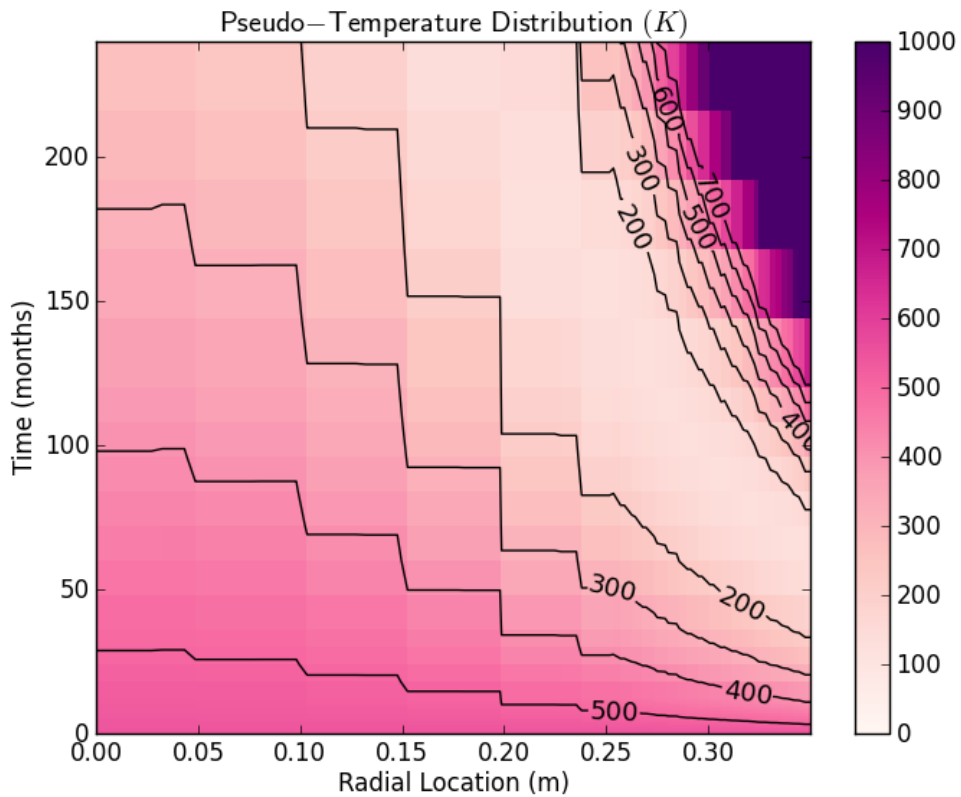
Figure 100: Pseudo Temperature Distribution Evolution at Z=275cm.

Looking at Figure 4.10, the surface plot of pseudo-temperature distribution over radius and time, it is evident that the innermost region of the central reflector

is heavily shielded from this type of fast neutron damage. Even at 240 months the innermost region has not reached maximum contraction, whereas at r=35cm, maximum contraction occurs at 55.8 months. The turnaround point occurs when the central reflector has passed the maximum cooling mark and returns to its original 540K, which occurs at 111.6 months at r=35cm. The turnaround point and point of maximum contraction are first reached at r=35 cm, so this radial location will be the most limiting for estimating the lifetime. Note also the distinct change in data resolution at the r = 25cm mark. This is where the MCNP5 mesh changed from a fine mesh (r = 25cm to r=35cm) to a coarse mesh. While this data is undoubtedly coarser, and thus less attractive for this analysis, it is also evident that the outermost 10cm of the central reflector at this location will be the most important for estimating the lifetime.
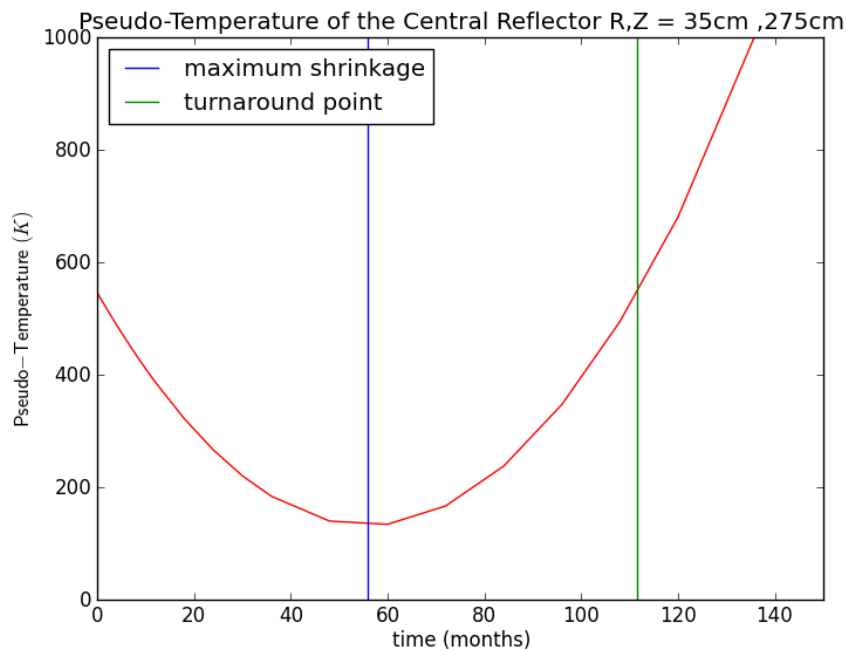
Figure 4.11: Plot of Pseudo Temperature evolution at a specific location on the central reflector. Vertical lines added to show intersection time of the point of maximum shrinkage and the turnaround point.

Recall that the Von Mises Stress sums the squares of the stress in each coordinate direction, and provides information on what tensile stress—compared to the one dimensional materials test—the material is undergoing. Accordingly, exceeding the ultimate tensile stress is the limiting factor in determining a lifetime estimate for the central reflector. Figure 4.12 illustrates the very evident deterioration of the central reflector, where the entire radial span from 0 to 35cm exceeds the UTS at t=50 months. As the UTS is around 25 MPa, the time at which the 2.5e7 contour line starts is the limited lifetime. From figure 4.13, this occurs at approximately 6.5 months.
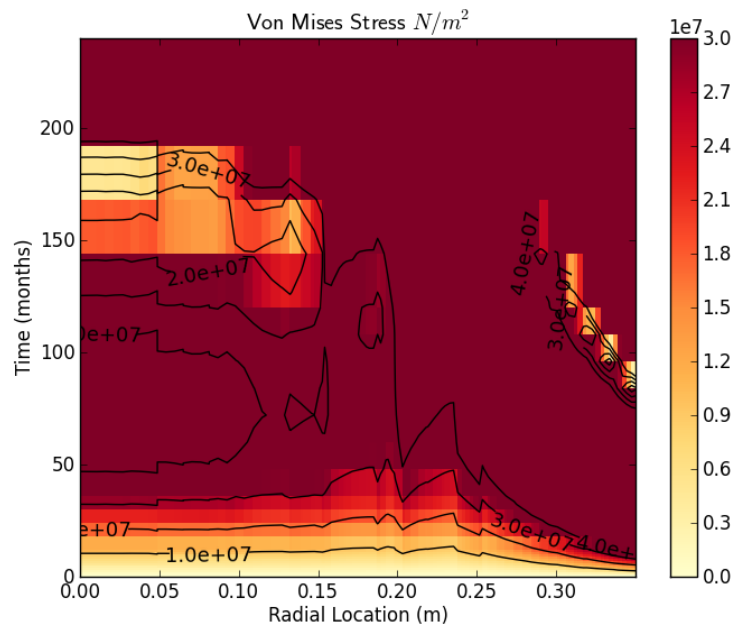
Figure 4.12: Von Mises Stress at z=275cm for the first 20 EFPY
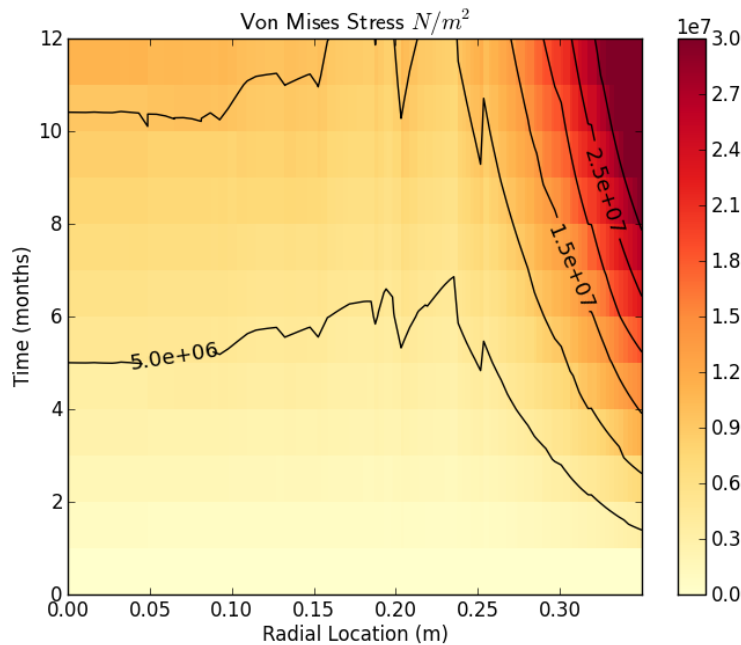
Figure 4.13: Von Mises Stress at z=275cm for the first 12 EFPM

The subsequent six surface plots (figs. 4.14-4.19) resolve the stress into each coordinate: R, Z and Phi. The colormap's extreme ends are close to the UTS of 25 MPA and UCS of 71MPA. Contour lines have been added to make this data more accessible. Solid lines indicate tensile stresses and dashed lines indicate compressive stresses. The earliest point at which the UCS or UTS occurs is the lifetime limiting time for the central reflector. The data was acquired from COMSOL

for the finest radial mesh at z=275cm, or the axial midplane of the central reflector. This is roughly the point with the highest fluence deposition rate, and thus the location at which the stress propagation will occur the fastest while not including the stress concentrating intersection points for the expansion and contraction regions of the core. The lifetimes estimates using only each resolved stress is summarized in Table 4.1.
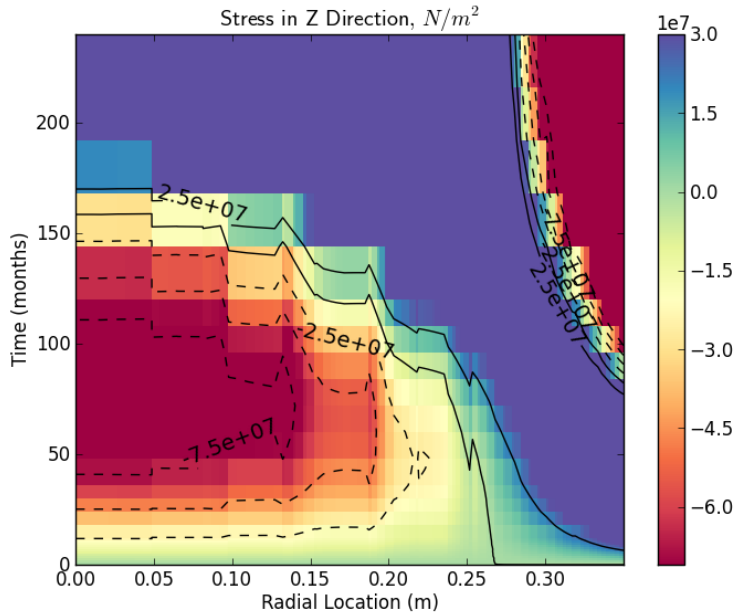
Figure 4.14: Resolved stress in Z coordinate only, at z=275 and for the first 20 EFPY.
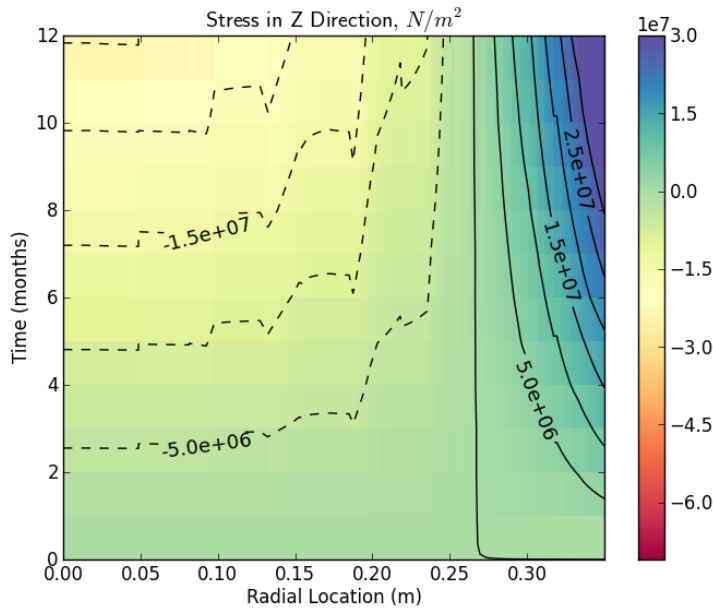
Figure 4.15: Resolved stress in Z coordinate only, at z=275 and for the first 12 EFPM.
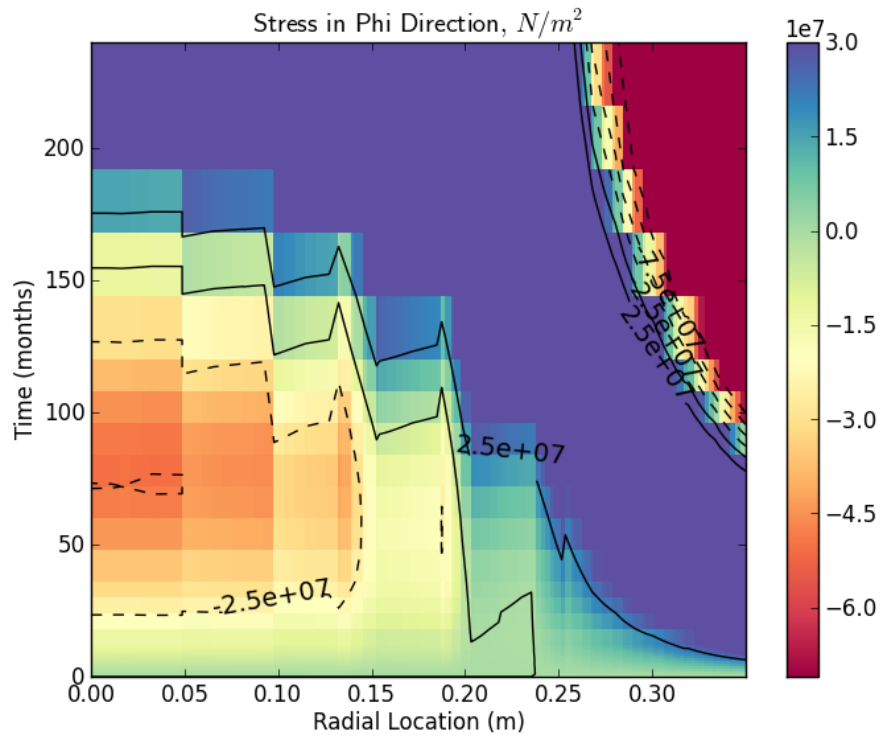
Figure 4.16: Resolved stress in Phi coordinate only, at z=275 and for the first 20 EFPY.
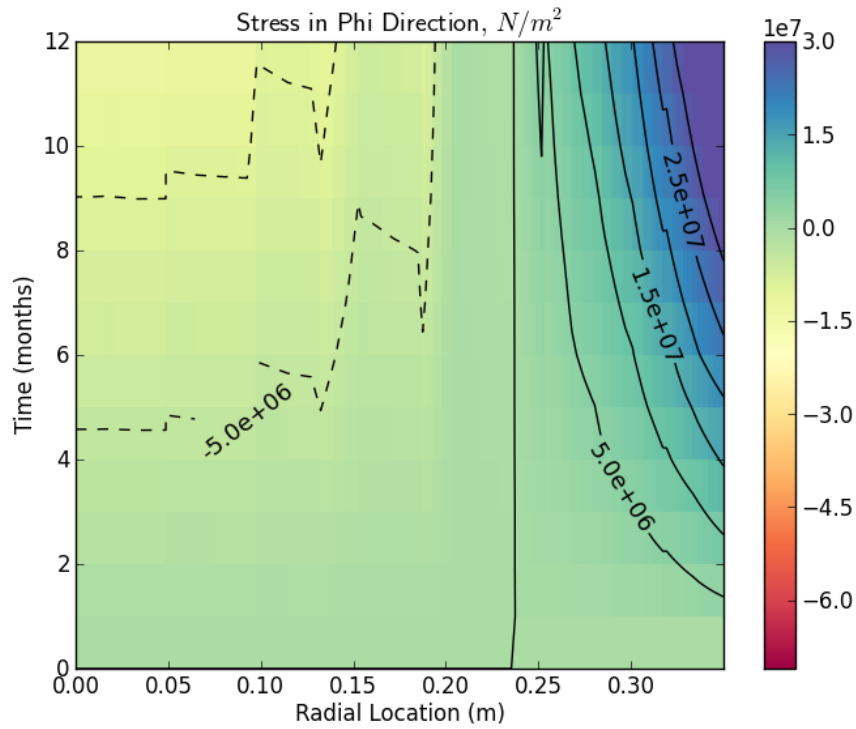
Figure 4.17: Resolved stress in Phi coordinate only, at z=275 and for the first 12 EFPM.
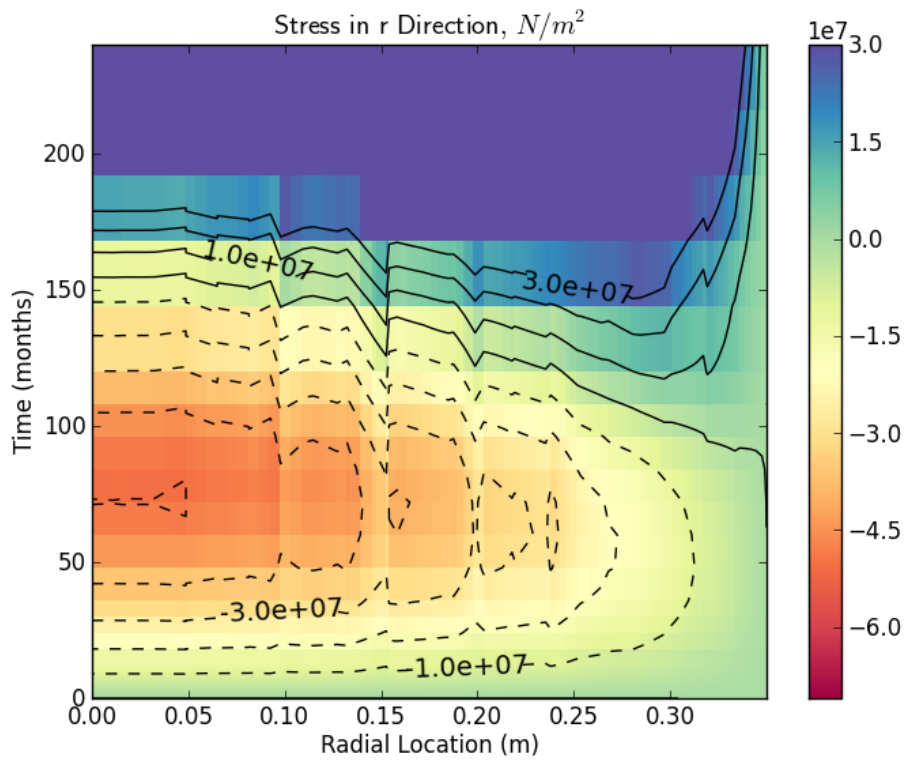
Figure 4.18: Resolved stress in R coordinate only, at z=275 and for the first 20 EFPY.
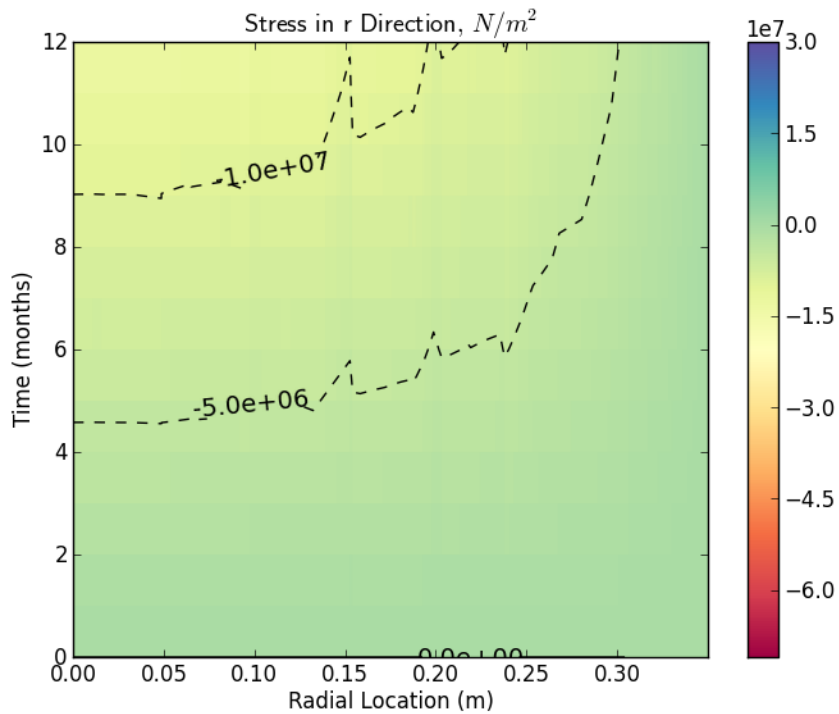
Figure 4.19: Resolved stress in R coordinate only, at z=275 and for the first 12 EFPM.
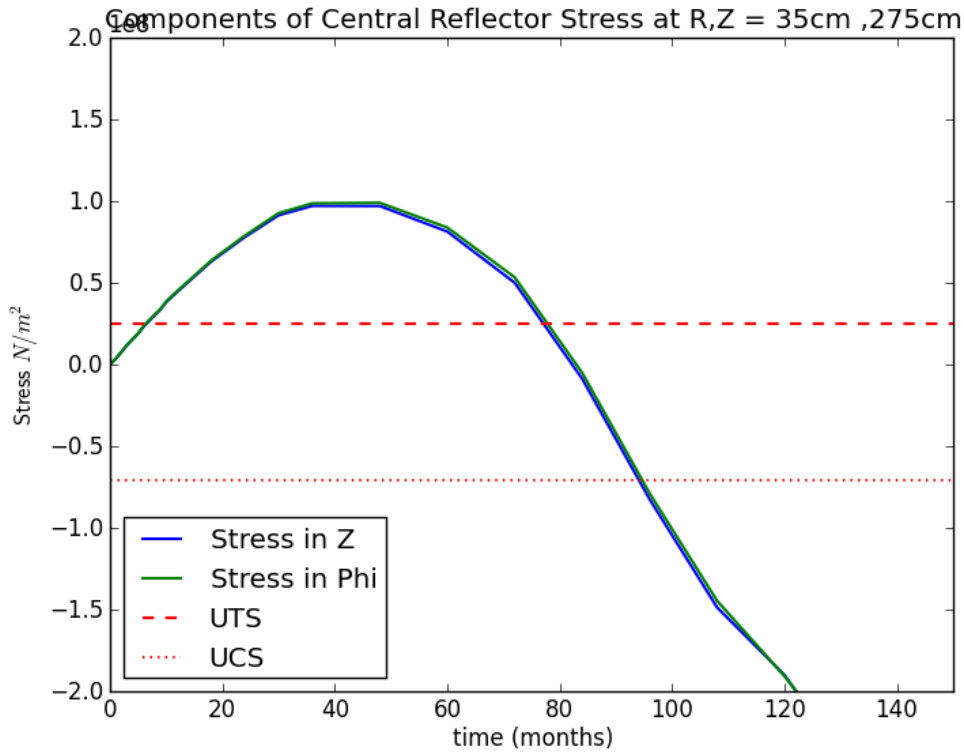
Figure 4.20: Z and Phi Resolved stresses at axial centerline and r=35cm. Ultimate tensile and compressive strengths are included with dashed and dotted red lines.

Lifetime Estimates With Different Failure Criteria		
Limiting Factor	Time (months)	Failure Type
Von Mises (Total Body)	4.2	--
Von Mises (R, Z = 35, 275)	6.5	--
Stress Phi	6.6	Tensile
Stress Z	6.7	Tensile
Stress R	142.2	Tensile
Turnaround Point	111.6	--
Maximum Contraction	55.8	--

Table 4.1: A comparison of different lifetime estimates with various limiting factors. Failure type of Von Mises is implicitly tensile, while failure types of turnaround and maximum contraction points are neither UTS nor UCS.

Table 4.1 condenses the data from section 4 into a table with various lifetime estimates for each marker described in the previous paragraphs. The Von Mises (Total Body) stress has the shortest lifetime estimate, which is expected, as stress buildup at the corners of the nonuniform geometry will shorten the lifetime. The subsequent Von Mises evaluation and the resolved stresses of Z and Phi are evaluated at the R = 35cm, Z=275cm location, as it is the point with the highest fluence in the central reflector that does not include the stress buildup at the

corners. This should give some indication of the lifetime of a large component central reflector with a uniform geometry, which may be representative of a central reflector constructed of large blocks of graphite. The lifetime estimates increase by a few months using the Von Mises criterion at this particular location rather than the full body. Figs 4.15 and 4.17 indicate that the 35 cm radial location is the first point at which the UTS is exceeded in the Z and Phi stress components, however, these two components have similar lifetime estimates to the Von Mises criterion. As such, it would be valuable to reconsider the central reflector geometry, and design it to resolve stresses in these components. Conversely, the radial stress coordinate is not limiting, and future design iterations do not require substantial stress relief for this stress component. The radial stress component provides, in fact, the longest lifetime estimate for the central reflector.

The lifetime of the reflector using the turnaround point and point of maximum contraction are also included in Table 4.1. The point of maximum contraction has nearly an order of magnitude longer lifetime than the Von Mises criterion, and the turnaround point overestimates the lifetime by an even greater amount. It is evident that neither of these criteria are conservative in terms of lifetime estimation, and should only be used on components with small fluence variation. These two factors should not be used in any situation where large reactor components see significant fast fluence depositions. Instead, a simulation like the one described in these pages would be more informative, safe, and conservative.

5. Conclusion

This study aimed to give a preliminary estimate of the lifetime of the graphite central reflector in the UCB PB-FHR reactor design. The central reflector was analyzed at various time increments, and it was found that the lifetime was much shorter than expected. With the current design, the central reflector will last between 6-7 effective full power months in the PB-FHR core, and even less if the Von Mises criterion over the entire central reflector is included. However, the lifetime limit can be extended if the central reflector is evaluated using only the radial component of the stress. While this is not physical, it provides an upper bound to the lifetime of future design iterations that relieve axial and azimuthal stresses.

The outermost edges of the central reflector at the axial centerline reach the turnaround point at 6.5 EFPY. Because there is close to an order of magnitude difference in the lifetime of the central reflector using the Von Mises criterion and the turnaround point method, it is evident that the turnaround point is not an effective metric for evaluating the lifetime of large reactor components in high fluence regions of the core. Additionally, a more conservative metric of limiting the lifetime to the point of greatest contraction also tends to overestimate the lifetime of the central reflector compared to the Von Mises criterion. For large components like the central reflector, a lifetime estimation method that incorporates the fluence and

stress distribution over the component will more conservatively determine the lifetime.

The lifetime of the PB-FHR central reflector is not acceptable at this time. A replacement frequency of 6 months would invalidate the advantageous design of the continuously refueled PB-FHR, requiring a period of shutdown every time the reflector is replaced. This reflector lifetime would, in all likelihood, render the PB-FHR a fiscally unachievable and unmarketable design. A redesign of the central reflector to optimize stress relief in the azimuthal and axial directions is required to make this reactor design realistic. This work was performed in a subsequent study using the same methodology outlined in this report [3]. The central reflector lifetimes with design alterations appeared to have beneficial effects.

6. Future Work

Future work on this project will involve design iterations of the central reflector to minimize radiation-induced stresses. This will include optimization of the height of each assembly block of the central reflector, the rounding of edges and corners (where stresses can concentrate), and also the quantity and dimensions of coolant channels in the periphery of the central reflector. Other possible iterations may include the choice of various NGGs, as only IG-110 was investigated here. Other NGGs may prolong the lifetime of the central reflector, and may be more useful in the case of the PB-FHR.

A more thorough stress analysis including loading from the coolant and pebbles will also be necessary in the future. However, based on the buoyantly loaded central reflector during full power operation, the stresses simulated in this approach—using gravity loads without flibe boundary conditions—shows that these stresses will be much smaller than those induced by the dimensional changes from radiation swelling.

Because the PB-FHR central reflector was limited by radiation-induced stresses in the azimuthal and axial directions, it would be of great interest to include axial and azimuthal segmentation in future iterations of the central reflector. A parametric study optimizing the height and angle at which these segmentations should occur would be of great benefit for not just the PB-FHR, but also other reactors using large graphite components in high-fluence regions of the core.

Additionally, it may be noted [31] that both the compressive and tensile loading failure is exhibited by nonlinear behavior. The work performed in this study utilized a linear elastic loading in order to use the pseudo-temperature distribution to simulate stress. Realistically, the material will exhibit this nonlinear behavior early in its lifetime, and this should be accounted for in a future study. However, the tensile failure will dominate in the central reflector, and the tensile loading appears to have a more linear-like behavior. The extent to which this will influence the results is probably not negligible, but still within an order of magnitude. As such, the conclusions reached by this study are not void, and a redesign to relieve radiation-induced dimensional changes is still necessary.

References

[1] Allen, Todd, Syd Ball, Edward Blandford, Thomas Downar, George Flanagan, Charles Forsberg, Ehud Greenspan, et al. "Fluoride-Salt-Cooled, High-Temperature Reactor (FHR) Subsystems Definition, Functional Requirement Definition, and Licensing Basis Event (LBE) Identification White Paper," 2013. http://fhr.nuc.berkeley.edu/wp-content/uploads/2013/08/12-001-FHR-Workshop-1-Report-Final.pdf.

[2] Allen, Todd, Edward Blandford, Guoping Cao, Douglas Chapin, Matthew Denman, Thomas Downar, George Flanagan, et al. "Fluoride-Salt-Cooled, High-Temperature Reactor (FHR) Methods and Experiments Program White Paper," 2013.

[3] Brigette Badro, Cameron Bailey, Stephen Kaplan, Hin Lee, and Mariam Malek, "NE-170 Applications of Finite Element Modeling (FEM) and Experiments to Study the Mk1 PB-FHR Center Reflector," Department of Nuclear Engineering, U.C. Berkeley, Report UCBTH-14-004, 2014.

[4] Boyd, R. W., and G. L. Fischer. *Encyclopedia of Materials: Science and Technology*. Elsevier Science Ltd, 2001.

[5] Bradford, Mark R., and Alan G. Steer. "A Structurally-Based Model of Irradiated Graphite Properties." *Journal of Nuclear Materials* 381, no. 1 (2008): 137–44.

[6] Brown, Forrest B., R. F. Barrett, T. E. Booth, J. S. Bull, L. J. Cox, R. A. Forster, T. J. Goorley, et al. "MCNP Version 5." *Trans. Am. Nucl. Soc* 87, no. 273 (2002): 02–3935.

[7] Burchell, T. D. "4.10 - Radiation Effects in Graphite." In *Comprehensive Nuclear Materials*, edited by Rudy J. M. Konings, 299–324. Oxford: Elsevier, 2012.

[8] ———. "Radiation Effects in Graphite and Carbon-Based Materials." *MRS Bulletin* 22, no. 04 (1997): 29–35.

[9] Burchell, T. D., W. P. Eatherly, J. M. Robbins, and J. P. Strizak. "The Effect of Neutron Irradiation on the Structure and Properties of Carbon-Carbon Composite Materials." *Journal of Nuclear Materials* 191 (1992): 295–99.

[10] Burchell, Timothy D. "Irradiation Induced Creep Behavior of H-451 Graphite." *Journal of Nuclear Materials* 381, no. 1 (2008): 46–54.

[11] Callister, William D., and David G. Rethwisch. *Materials Science and Engineering: An Introduction*. Vol. 7. Wiley New York, 2007.

[12] Cisneros Jr, Anselmo Tomas. "Pebble Bed Reactors Design Optimization Methods and Their Application to the Pebble Bed Fluoride Salt Cooled High Temperature Reactor (PB-FHR)." PhD Dissertation, UNIVERSITY OF CALIFORNIA, BERKELEY, 2013.

[13] Comsol, A. B. "COMSOL Multiphysics User's Guide." *Version: September*, 2005.

[14] Davies, Mark A., and Mark Bradford. "A Revised Description of Graphite Irradiation Induced Creep." *Journal of Nuclear Materials* 381, no. 1 (2008): 39–45.

[15] Facilitators, M. I. T., and UW Madison Facilitators. "Fluoride-Salt-Cooled, High-Temperature Reactor (FHR) Development Roadmap and Test Reactor Performance Requirements White Paper," 2013. http://fhr.nuc.berkeley.edu/wp-content/uploads/2013/08/12-004-FHR-Workshop-4-Report-Final.pdf.

[16] Facilitators, UW Madison, and M. I. T. Facilitators. "Fluoride-Salt-Cooled High Temperature Reactor (FHR) Materials, Fuels and Components White Paper," 2013. http://fhr.nuc.berkeley.edu/wp-content/uploads/2013/08/12-003-FHR-Workshop-3-Report-Final.pdf.

[17] Golubov, S. I., A. V. Barashev, and R. E. Stoller. "1.13 - Radiation Damage Theory." In *Comprehensive Nuclear Materials*, edited by Rudy J. M. Konings, 357–91. Oxford: Elsevier, 2012.

[18] Ishiyama, S., T. D. Burchell, J. P. Strizak, and M. Eto. "The Effect of High Fluence Neutron Irradiation on the Properties of a Fine-Grained Isotropic Nuclear Graphite." *Journal of Nuclear Materials* 230, no. 1 (1996): 1–7.

[19] Kelly, B. T., and T. D. Burchell. "The Analysis of Irradiation Creep Experiments on Nuclear Reactor Graphite." *Carbon* 32, no. 1 (1994): 119–25.

[20] Kelly, B. T., and A. J. E. Foreman. "The Theory of Irradiation Creep in Reactor graphite—The Dislocation Pinning-Unpinning Model." *Carbon* 12, no. 2 (1974): 151–58.

[21] Krumwiede, David L., Charalampos Andreades, Anselmo T. Cisneros, Jeffrey E. Seifried, Raluca O. Scarlat, Nicolas Zweibaum, Ehud Greenspan, and Per F. Peterson. "Design of a Pre-Conceptual Pebble-Bed, Fluoride-Salt-Cooled, High-Temperature Reactor Commercial Power Plant." In *Proceedings of ICAPP 2014*. Charlotte, NC, 2014.

[22] Krumwiede, David L., Raluca O. Scarlat, J.K. Choi, T.M. Phan, and Per F. Peterson. "Three-Dimensional Modeling of the Pebble-Bed Fluoride-Salt-Cooled, High-

Temperature Reactor (PB-FHR) Commercial Plant Design." In *Proceedings of the American Nuclear Society 2013 Winter Meeting*, 2013.

[23] Lemaignan, Clément. "Nuclear Materials and Irradiation Effects." In *Handbook of Nuclear Engineering*, 543–642. Springer, 2010. http://link.springer.com/10.1007/978-0-387-98149-9_6.

[24] Lommers, Lew, and George Honma. *NGNP High Temperature Materials White Paper*. Idaho National Laboratory (INL), 2012. http://www.osti.gov/scitech/biblio/1055953.

[25] Marsden, B. J., and G. N. Hall. "4.11 - Graphite in Gas-Cooled Reactors." In *Comprehensive Nuclear Materials*, edited by Rudy J. M. Konings, 325–90. Oxford: Elsevier, 2012.

[26] Maruyama, Tadashi, and Masaaki Harayama. "Neutron Irradiation Effect on the Thermal Conductivity and Dimensional Change of Graphite Materials." *Journal of Nuclear Materials* 195, no. 1 (1992): 44–50.

[27] Mohanty, S., and S. Majumdar. "HTGR Graphite Core Component Stress Analysis Research Program–Task 1 Technical Letter Report." *Argonne National Laboratory*, 2011.

[28] Oku, Tatsuo, and Masahiro Ishihara. "Lifetime Evaluation of Graphite Components for HTGRs." *Nuclear Engineering and Design* 227, no. 2 (2004): 209–17.

[29] Olander, Donald R. *Fundamental Aspects of Nuclear Reactor Fuel Elements*. California Univ., Berkeley (USA). Dept. of Nuclear Engineering, 1976.

[30] Scarlat, Raluca O., Michael R. Laufer, Edward D. Blandford, Nicolas Zweibaum, David L. Krumwiede, Anselmo T. Cisneros, Charalampos Andreades, et al. "Design and Licensing Strategies for the Fluoride-Salt-Cooled, High-Temperature Reactor (FHR) Technology." *Progress in Nuclear Energy*. Accessed September 3, 2014. doi:10.1016/j.pnucene.2014.07.002.

[31] Shibata, Taiju, Kazuhiro Sawa, Motokuni Eto, Eiji Kunimoto, Shusaku Shiozawa, Tatsuo Oku, and Tadashi Maruyama. *Draft of Standard for Graphite Core Components in High Temperature Gas-Cooled Reactor*. Japan Atomic Energy Agency, Tokai, Ibaraki (Japan), 2010.

[32] Tsang, D. K. L., and B. J. Marsden. "Effects of Dimensional Change Strain in Nuclear Graphite Component Stress Analysis." *Nuclear Engineering and Design* 237, no. 9 (2007): 897–904.

[33] ———. "The Development of a Stress Analysis Code for Nuclear Graphite Components in Gas-Cooled Reactors." *Journal of Nuclear Materials* 350, no. 3 (2006): 208–20.

[34] Zweibaum, Nicolas, Guoping Cao, Anselmo T. Cisneros, Brian Kelleher, Michael R. Laufer, Raluca O. Scarlat, Jeffrey E. Seifried, et al. "Phenomenology, Methods and Experimental Program for Fluoride-Salt-Cooled, High-Temperature Reactors (FHRs)." *Progress in Nuclear Energy*, 2014.